

---

Masters Theses

Student Theses and Dissertations


---

1972

## Computer simulation of the primary recoil spectra and damage cross section of Fe<sub>3</sub>Al using ENDF/B II data

Daniel Willard Smith

Follow this and additional works at: [https://scholarsmine.mst.edu/masters\\_theses](https://scholarsmine.mst.edu/masters_theses)

 Part of the [Nuclear Engineering Commons](#)

Department:

---

### Recommended Citation

Smith, Daniel Willard, "Computer simulation of the primary recoil spectra and damage cross section of Fe<sub>3</sub>Al using ENDF/B II data" (1972). *Masters Theses*. 3539.  
[https://scholarsmine.mst.edu/masters\\_theses/3539](https://scholarsmine.mst.edu/masters_theses/3539)

This thesis is brought to you by Scholars' Mine, a service of the Curtis Laws Wilson Library at Missouri University of Science and Technology. This work is protected by U. S. Copyright Law. Unauthorized use including reproduction for redistribution requires the permission of the copyright holder. For more information, please contact [scholarsmine@mst.edu](mailto:scholarsmine@mst.edu).

COMPUTER SIMULATION OF THE PRIMARY RECOIL SPECTRA AND  
DAMAGE CROSS SECTION OF Fe<sub>3</sub>A1 USING ENDF/B II DATA

BY

DANIEL WILLARD SMITH, 1947-

A THESIS

Presented to the Faculty of the Graduate School of the

UNIVERSITY OF MISSOURI-ROLLA

In Partial Fulfillment of the Requirements for the Degree

MASTER OF SCIENCE IN NUCLEAR ENGINEERING

1972

T2827  
80 pages  
c.1

Approved by

H. P. Leighty, Jr. (Advisor) D. Ray Edwards  
Edward B. Hale

## ABSTRACT

A computer program, using Evaluated Nuclear Data File (ENDF/B II) information, was used to develop energy-exchange kernels which delineate the energy transfer probabilities between neutrons and  $\text{Fe}_3\text{Al}$  lattice atoms. The kernels combine all available information on elastic and inelastic scattering contained in the ENDF/B II data.

The computer program used to generate the primary recoil spectra is SAKI, a modified version of RICE (1). SAKI is designed to calculate energy-exchange probabilities in any binary alloy as well as damage cross sections and optimum cutoff energies for use in comparing displacement effects in different reactor spectra.

## ACKNOWLEDGEMENT

The author sincerely wishes to express his gratitude to both Dr. H. P. Leighly, Jr., Professor of Metallurgical Engineering, and Dr. D. R. Edwards, Associate Professor of Nuclear Engineering for their help, advice, suggestions, and encouragement in preparing this thesis.

A special expression of thanks to Mr. J. D. Jenkins of Oak Ridge National Laboratory for the computer code RICE, the ENDF/B libraries, and valuable correspondence.

In addition, the author wishes to express his appreciation to the U.M.R. Computer Science Center for furnishing the computer facilities, and to Glenn W. Schade, Graduate Student in Nuclear Engineering, for his help in computer programming as well as valuable discussion.

## TABLE OF CONTENTS

	Page
ABSTRACT.....	ii
ACKNOWLEDGEMENT.....	iii
LIST OF FIGURES.....	vi
I. INTRODUCTION.....	1
II. REVIEW OF LITERATURE.....	2
A. THE ORDERED ALLOY SYSTEM.....	2
B. THE ORDER-DISORDER ALLOY - $Fe_3Al$ .....	7
C. RADIATION DAMAGE TO ORDERED ALLOYS.....	13
D. RADIATION DAMAGE TO $Fe_3Al$ .....	16
E. RADIATION DAMAGE COMPUTER STUDIES INCLUDING $Fe_3Al$ .....	18
III. COMPUTATIONAL PROCEDURE.....	26
A. INTRODUCTION.....	26
B. CALCULATION OF THE ENERGY TRANSFER KERNEL.....	26
C. PRIMARY RECOIL ATOM SPECTRA.....	32
D. DAMAGE CROSS SECTIONS AND ENERGY CUTOFFS.....	32
E. COMPOUND CALCULATIONS.....	33
IV. COMPUTATIONAL RESULTS.....	36
A. DAMAGE CROSS SECTION FOR $Fe_3Al$ .....	36
B. PRIMARY RECOIL ATOM SPECTRA.....	40
V. DISCUSSION OF RESULTS.....	43
VI. CONCLUSIONS.....	51
VII. RECOMMENDATIONS.....	53
BIBLIOGRAPHY.....	54

Table of Contents (continued)	Page
VITA.....	57
APPENDICES.....	58
A. COMPUTER INPUT DATA.....	58
B. DAMAGE CROSS SECTIONS OF IRON, ALUMINUM, AND Fe <sub>3</sub> Al CALCULATED FROM SAKI.....	64
A. Total Damage Cross Sections.....	64
B. Inelastic Damage Cross Sections.....	67
C. ENERGY DISTRIBUTION OF Fe <sub>3</sub> Al RECOIL ATOMS FROM TWO NEUTRON SPECTRA.....	69
D. IRON DAMAGE CROSS SECTIONS AS DETERMINED BY SAKI, JENKINS, AND DORAN.....	71

## LIST OF FIGURES

Figure	Page
1. $\text{Fe}_3\text{Al}$ ( $\text{DO}_3$ ) Superlattice.....	8
2. Resistivity vs. Temperature for Ordered and Disordered $\text{Fe}_3\text{Al}$ as Determined by Bennet [11].....	10
3. Resistivity vs. Temperature upon Slow Cooling of $\text{Fe}_3\text{Al}$ as Determined by Rauscher [12].....	11
4. Equilibrium Degree of Long Ranged Order in $\text{Fe}_3\text{Al}$ as a Function of Temperature as Reported by Rauscher [12].....	12
5. Two Representative Neutron Spectra Used in SAKI Calculations.....	27
6. Iron Damage Cross Sections Calculated by SAKI.....	37
7. Aluminum Cross Sections Calculated by SAKI.....	38
8. Damage Cross Sections of $\text{Fe}_3\text{Al}$ Calculated by SAKI.....	39
9. Energy Distribution of $\text{Fe}_3\text{Al}$ Recoil Atoms from Two Neutron Spectra.....	41
10. Comparison of Iron Damage Cross Sections from ENDF/B Data as Calculated by Jenkins [29] with Results Published by Sheely [35].....	47
11. Comparison of Iron Damage Cross Sections from ENDF/B Data as Calculated by Jenkins [29] with Results Published by Doran [31].....	48

## I. INTRODUCTION

Since the discovery of radiation, man has inquired into the effects of this radiation on his environment. Even before the advent of the nuclear reactor, many studies were undertaken to provide a greater insight concerning radiation induced effects and mechanisms in solids.

With the discovery of radiation, a keen interest developed concerning its effects on order-disorder alloys.

Utilizing the computer as the tool of investigation, this research will determine the primary recoil atom spectra and damage cross section of the ordered  $\text{Fe}_3\text{Al}$  alloy.

The primary recoil atom spectra can be helpful in predicting the size distribution of displacement spikes and calculations concerning the formation of voids in irradiated materials in a particular neutron environment.

Damage cross sections are a measure of the number of displacements produced in the irradiated solid per atom site and is independent of the neutron flux spectra in a reactor system. SAKI utilizes ENDF/B cross section data and the Kinchin-Pease model [2] for the displacements produced per primary knock-on atom.



## II. REVIEW OF LITERATURE

The following is a review of the many investigations concerning the order-disorder phenomena, the alloy  $\text{Fe}_3\text{Al}$ , and the effects of radiation bombardment on  $\text{Fe}_3\text{Al}$ . Also included are various computer studies.

### A. THE ORDERED ALLOY SYSTEM

An alloy composed of A atoms and B atoms is said to be ordered if the composition of the alloy can be expressed in a stoichiometrically simple formula AB or  $\text{AB}_3$  (or very near to these ratios) and if the atoms occupy specific lattice sites in the crystal structure [3]. When the alloy has become ordered in some region or "domain" then it is said to have acquired a "superlattice" which describes its geometric arrangement.

Most of the experimental data on ordering have come from x-ray diffraction studies or diffraction contrast in the electron microscope [4]. The Fourier transform of the alloy's diffraction pattern (the Patterson function) describes the probability of finding one atom type at some interatomic vector from another. First, neglecting the fact that if the different atoms have different sizes in the solid solution, each pair may be at a slightly different interatomic vector. Assume a binary alloy composed of A solute atoms and B solvent atoms. The Patterson function becomes

$$P(\bar{r}) = N \left\{ (x_A Z_A + x_B Z_B)^2 + x_A x_B (Z_A - Z_B)^2 \left[ 1 - \frac{p_{jk}^B | A}{x_B} \right] \right\} \quad (1)$$

where

$N$  = the total number of A and B atoms

$Z_i$  = the atomic number of  $i$

$x_i$  = the fraction of  $i$  atoms in the composition

$P_{j|k}^{B|A}$  = the conditional probability that there is a B atom at site  $j$  if there is an A atom at  $k$

$$x_A + x_B = 1$$

The Patterson function is composed of two terms. The first is much larger than the second and depends on the alloy's average structure. It is derived from fundamental peaks of the Fourier transform and is not affected by changes in atomic arrangement excluding interatomic distance changes and changes in the vibrational spectrum. The second term describes local or short ranged order. The term

$$\left[ 1 - \frac{P_{j|k}^{B|A}}{x_B} \right]$$

is referred to as  $\alpha_{lmn}$ , the Warren local order coefficient. The coordinates of the interatomic vector between sites  $j, k$  are  $lmn$ . If the alloy is completely random then  $\alpha_{lmn}$  is zero. The absolute value of  $\alpha_{lmn}$  also cannot exceed one. Its maximum negative value occurs at  $\alpha_{lmn} = 1 - (1/x_B)$ , when the atomic fraction is that of the solvent B atoms. If the A atoms and B atoms have close atomic numbers then it is difficult to detect diffuse scattering from local order using x-rays. Also, there are numerous effects that arise in diffraction patterns due to the fact that in close-packed solid solutions atoms of different sizes may not be exactly at lattice points. Examples may be modulation of the diffuse scattering or peak depressions. These are dependent on

the state of local order. It is possible, however, to detect local "changes" in atomic arrangement even though the atomic numbers of the A atoms and B atoms differ only slightly. Experimental work has been done to determine the Warren local order coefficient. It is determined by transforming the diffuse intensity measured in a repeated volume of reciprocal space after being corrected for effects due to atomic size, temperature, parasitic scattering due to air and equipment, and Compton scattering.

The parameter  $S$  is a measure of long range order. When  $S = 1$  the alloy is completely ordered and when  $S$  is zero, the alloy is completely disordered. The critical temperature of the alloy,  $T_c$ , is the characteristic temperature at which complete disordering occurs. For example, assume that a completely ordered alloy is gradually heated. As the temperature of the alloy is raised the amplitude of thermal vibrations of the atoms about their equilibrium positions is greater. When these vibrations become large enough, there may be an interchange of atoms causing some disorder introduced into the superlattice. Disordering will increase with temperature until, at some critical temperature of the alloy, the superlattice disappears entirely. Some local order will still exist due to attraction of unlike atoms. Upon cooling at a temperature above  $T_c$ , the events occur in reverse. At absolute zero the alloy will acquire perfect order. The long range order parameter was originally proposed by Bragg and Williams [5] as a linear function of the fraction of sites of one sublattice which is occupied by the "correct" atoms -- those that occupy the sublattice at total order.

$$S = a + br_{\alpha} \quad (2)$$

where  $r_{\alpha}$  is the fraction of  $\alpha$  sublattice occupied by right atoms.

Let

$x_A$  = the molar fraction of A atoms in the alloy

$x_B$  = the molar fraction of B atoms in the alloy

$w_{\alpha}$  = the fraction of  $\alpha$  sublattice occupied by wrong atoms

$w_{\beta}$  = the fraction of  $\beta$  sublattice occupied by wrong atoms

$r_{\beta}$  = the fraction of  $\beta$  sublattice occupied by right atoms

There may be a need for more than one order parameter in this description, however. For instance,  $\text{Fe}_3\text{Al}$  has a  $\text{DO}_3$  type superlattice structure which is composed of eight body centered cubic cells. One order parameter may be needed to describe the order between sites at corners, another for the center of the cells, and another for the iron and aluminum atoms on the body centered lattice points. However, the overall long range order parameter may be written as

$$S = \frac{r_{\alpha} - x_A}{1 - x_A} = \frac{r_{\beta} - x_B}{1 - x_B} \quad (3)$$

For the  $\text{Cu}_3\text{Au}$  system

$$S = (4/3)(r_{\alpha} - \frac{1}{4}) = 4(r_{\beta} - \frac{3}{4})$$

The face centered cubic  $\text{Cu}_3\text{Au}$  alloy has four sublattices, three equivalent ones occupied by copper atoms at full order ( $\beta$  sites at cube faces) and one sublattice occupied by gold atoms ( $\alpha$  sites at cube corners). A number of assumptions have to be made concerning this definition. The alloy must be described by a stoichiometric formula  $\text{AB}$  or  $\text{AB}_3$ . The ordered domains of the alloy must not be "out of phase"

with each other. An example of this may be that A atoms occupy one sublattice in one domain, another in an adjacent domain, and so on.

Cowley [6] has investigated free energies by the bond-energy approach in terms of the measurable local order parameters. His investigations along with the studies of Clapp and Moss [7] were on the face centered cubic alloy,  $\text{Cu}_3\text{Au}$ . They found the configurational energy,  $H$ , to be

$$H = \frac{N x_A x_B}{8 \pi^3} \sum_j A_j V(K_j) \quad (4)$$

where

$A_j$  = is proportional to the square of the structure factor for the superlattice reflections that appear at  $K_j$  in reciprocal space

$V(K_j)$  = the Fourier transform of the pair potentials where  $K_j$  is a position in reciprocal space

The configurational energy, thus, is a minimum for some atomic arrangement for which the  $K_j$  are at the minima of the  $V(K)$  spectrum.

$$V(K) = \sum_{lmn} V_{lmn} \exp(2\pi i \bar{p} \cdot \bar{r}_{lmn}) \quad (5)$$

$$\bar{p} = h_1 \bar{b}_1 + h_2 \bar{b}_2 + h_3 \bar{b}_3$$

where

$\bar{b}_i$  = the axes of the unit cell in reciprocal space

$h_i$  = continuous variables

For cubic metals or alloys

$$V(K) = \sum_{lmn} V_{lmn} \cos \pi l h_1 \cos \pi m h_2 \cos \pi n h_3 \quad (6)$$

The critical temperature can be defined for some  $K = K_m$  as

$$1 = - \frac{2 x_A x_B V(K_m)}{k T_c} \quad (7)$$

where  $k$  is the Boltzmann constant.

There have been a number of computer experiments on generating the ordered state by a "monte carlo" type procedure, mainly for face centered cubic alloys. Fosdick, Flinn, and Guttman [8-10] allowed an exchange of randomly chosen pairs of AB atoms creating wrong pairs according to a probability based on a Boltzmann weighing factor. Results for  $\text{Cu}_3\text{Au}$  [8] were encouraging up to  $T_c$ . Around the critical temperature their model was inappropriate and a larger model was needed. Difficulty was encountered when they attempted to simulate order for a body centered cubic type structure.

#### B. THE ORDER-DISORDER ALLOY - $\text{Fe}_3\text{Al}$

The superlattice structure of  $\text{Fe}_3\text{Al}$  is the  $\text{DO}_3$  type shown in figure 1. It is composed of eight body centered cubic cells and the iron and aluminum atoms occupy specific lattice sites within the superlattice.

Proper heat treatment is needed to insure ordering of the disordered phase. Slow cooling from a temperature well above  $T_c$  will allow the iron and aluminum atoms to select their specific sites in the crystal lattice. Rapid cooling or quenching will result in a B2 or disordered phase.

The effect of ordering on an alloy can be derived from electrical resistivity measurements at selected temperatures. A perfectly periodic lattice structure theoretically will have zero resistance.

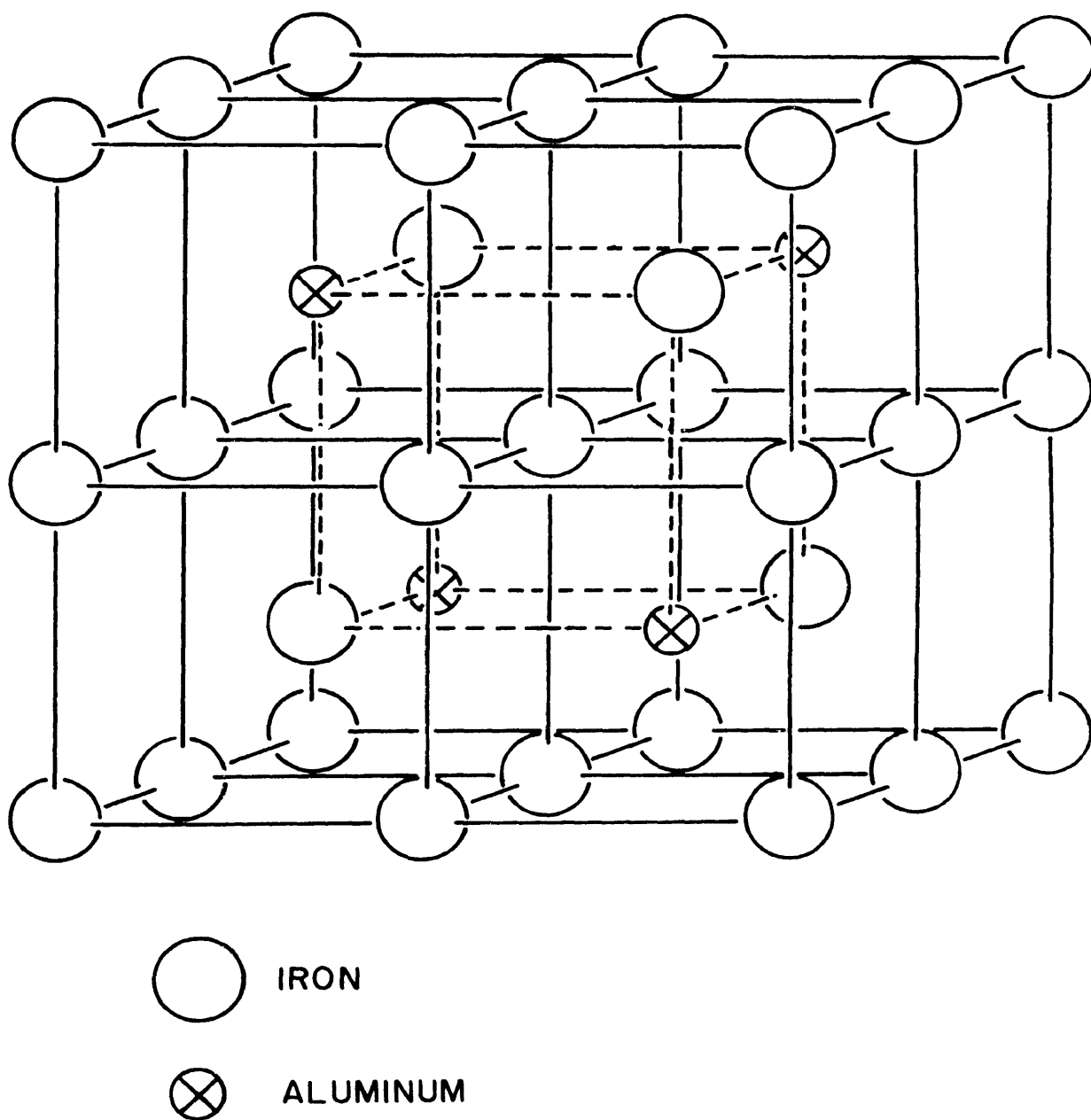


Figure 1.  $\text{Fe}_3\text{Al}$  ( $\text{DO}_3$ ) Superlattice

Any departure from perfect periodicity will result in an increase in electrical resistance. Therefore, there should be a marked decrease in resistivity upon ordering. Bennet [11] studied this effect on  $\text{Fe}_3\text{Al}$  as a function of temperature and various cooling rates. Results of his studies are shown in figure 2. As expected, the ordered specimen recorded a lower resistivity at low temperatures. Both the ordered and disordered alloys increased in resistivity as the temperature increased until they both converged at  $T_c$ . Rauscher [12] also investigated ordering in  $\text{Fe}_3\text{Al}$ . His slow cooling curve of resistivity as a function of temperature is shown in figure 3. He determined the critical temperature of the alloy to be around  $540^\circ\text{C}$ . This was accomplished by studying the long range order parameter as a function of temperature as shown in figure 4. The temperature at which the parameter becomes zero was defined to be the critical temperature.

Leamy, Gibson, and Kayser [13] investigated the elastic stiffness coefficients of iron-aluminum alloys. At about 25.05 atomic percent aluminum, the density was found to be  $6.6436 \text{ g/cm}^3$  and the interpolated lattice parameter,  $a_0$ , was 2.8964 angstroms.

Wert and Cupschalk [14] using electron microscopy studied the antiphase domain structure of  $\text{Fe}_3\text{Al}$ . Rapidly quenched specimens exhibited an extremely fine antiphase domain structure which increased with subsequent annealing. Marchinkowski and Brown [15] also found that the B2 and  $\text{D0}_3$  structures of  $\text{Fe}_3\text{Al}$  could coexist. They observed the antiphase boundaries which separate the two coexisting structures. The antiphase boundaries in both the imperfect B2 and  $\text{D0}_3$  type lattices showed no preference for any particular crystallographic planes. No



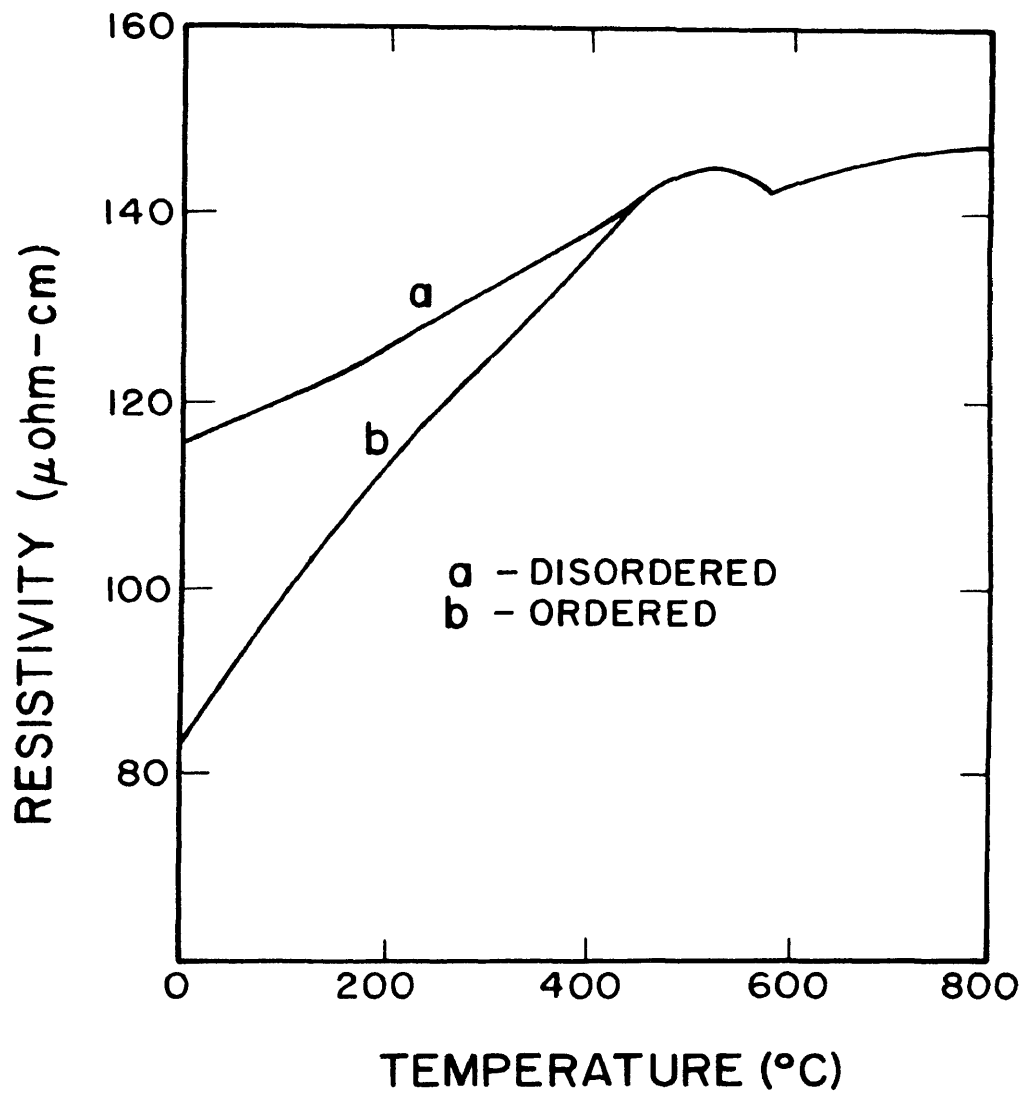


Figure 2. Resistivity vs. Temperature for Ordered and Disordered  $\text{Fe}_3\text{Al}$  as determined by Bennet [11].

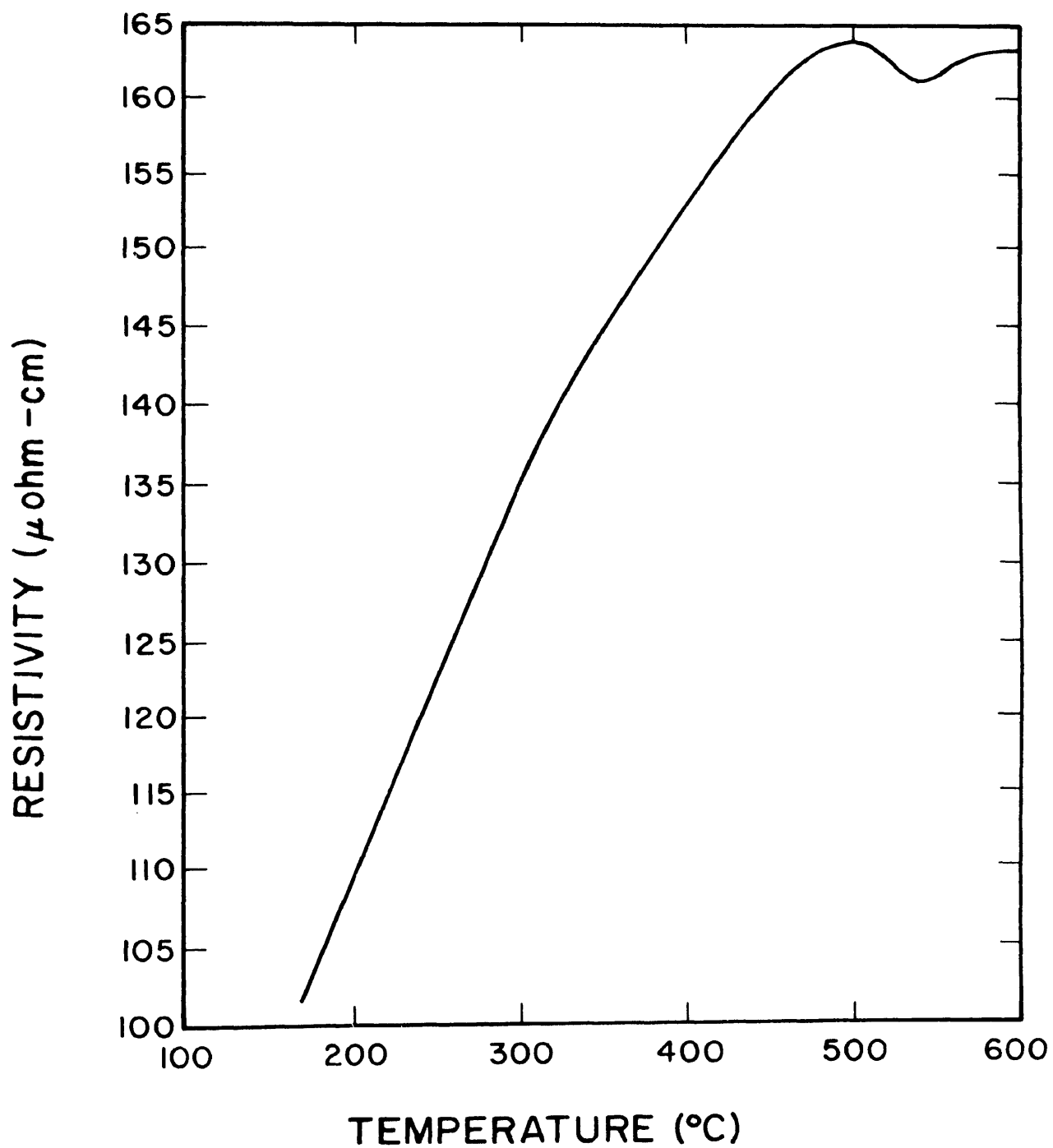


Figure 3. Resistivity vs. Temperature upon Slow Cooling of Fe<sub>3</sub>Al as determined by Rauscher [12].

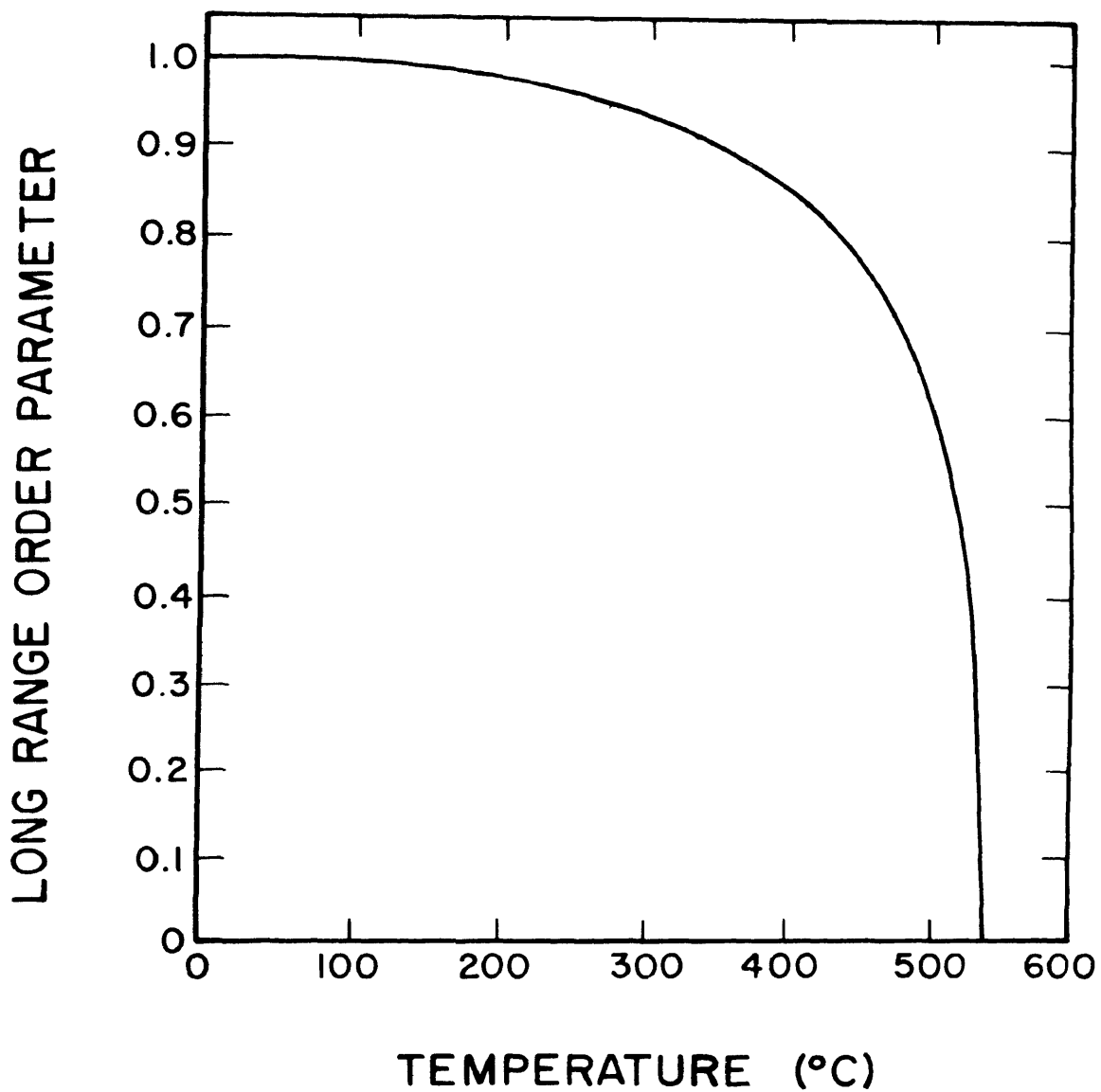


Figure 4. Equilibrium Degree of Long Ranged Order in  $\text{Fe}_3\text{Al}$  as a Function of Temperature as Reported by Rauscher [12].<sup>3</sup>

quenching rate was found to be fast enough to prevent the formation of the B2 structure. They also found that  $DO_3$  domains can form within existing and larger B2 type domains.

### C. RADIATION DAMAGE TO ORDERED ALLOYS

Because of the great difference in electrical properties between the ordered and disordered state, these alloys are well suited for radiation damage studies. Bombardment by high energy particles on the crystal lattice of the alloy will cause displacements if the particles impart sufficient energy to the target atoms [16]. The particles, first, will expend their energy by excitation with both conduction electrons and inner electrons of the atomic shells. Secondly, the particles transfer their energy to the lattice atoms by collision. The relative role of both processes will depend on the magnitude of the parameter,  $\epsilon$ , defined as

$$\epsilon = \frac{m_e}{M} E \quad (8)$$

where

$m_e$  = the mass of the electron

$M$  = the mass of the heavy particle

$E$  = the kinetic energy of the heavy particle, eV

For relatively large values of  $\epsilon$ , the first process will predominate. The energy transferred to the electrons is much greater than the energy given to the lattice atoms. The electrons subsequently will transfer energy to the alloy by interaction with the lattice atoms, thus heating of the crystal. For sufficiently lower values of  $\epsilon$ , the energy of the fast particles is transferred primarily to the lattice

atoms, thus, the second process predominates. If this energy is not sufficient to move a lattice atom from its equilibrium position, only vibrations of the crystal lattice atoms are excited. For larger energies, displacements will occur creating vacancies and interstitials. When a very large energy is given to the lattice atoms, the atoms travel rapidly through the crystal, exciting the same type of defects as the original particles. A number of vacancy-interstitial defects are also created in the region of the crystal which adjoins the trajectory of the fast particles. The liberation of energy in this region will cause a rather large increase in temperature and may result in melting. Rapid cooling of the region occurs because of good thermal transfer with the surroundings. In this way a disordered phase may be created and subsequently retained in an ordered alloy due to irradiation with fast particles.

A number of conclusions can be derived from experimental results on an order-disorder alloy [17]. The rate of ordering in an alloy increases with instantaneous flux and increases with temperature. The degree of ordering previously obtained decreases with increasing instantaneous flux and increases with increasing temperature. After a low or room temperature irradiation, there may be no observable change in order, but for subsequent annealing at room temperature or higher, some ordering of the alloy occurs. There seems to be a competition between the ordering and disordering processes during irradiation. The disordering process may result from a replacement mechanism, thermal spikes, or displacement spikes. The ordering process is due to migration of those simple defects which may produce

interchange of lattice atoms, the most obvious being the vacancy. During a high temperature irradiation and after a transitional state, the vacancy concentration is constant due to the equal number of vacancies produced and annihilated. For an interstitial-vacancy annihilation, the vacancy concentration increases as the square root of the instantaneous flux, therefore causing the rate of ordering to also increase with the flux. The same conclusion may be obtained by assuming enhanced diffusion caused by an interstitial mechanism, but the interstitial must migrate by a replacement mechanism and not be jumping from one interstitial site to a neighboring one.

Since neutrons interact very weakly with electrons most of their energy is transferred to the lattice atoms along their trajectory [16]. Local heating and lattice defects may occur due to neutron bombardment. The local heating may change the state of ordering and the lattice defects will accelerate the process of approaching the state of equilibrium at a given temperature. A relatively small number of defects are formed during electron bombardment. The incident electrons transfer most of their energy to the conduction and inner electrons of the atomic shells, and not to the crystal lattice atoms. In  $\gamma$ -ray bombardment, energy transfer with the electrons also occurs. Fast electrons are formed as a result of the Compton effect and the internal photoelectric effect. These fast electrons will interact with other electrons in the same manner as the primary electrons during irradiation.

#### D. RADIATION DAMAGE TO $\text{Fe}_3\text{Al}$

Saenko [18] studied the effects of neutron irradiation on  $\text{Fe}_3\text{Al}$  using fluences up to about  $10^{20} \text{ n/cm}^2$ . The effect on neutron bombardment at a temperature of about  $80^\circ\text{C}$  in both the annealed and quenched states were investigated by measuring electrical resistivity, crystal lattice parameter and the intensity of superstructural lines from x-ray diffraction patterns. He found that the superlattice diffraction lines decreased and ultimately vanished due to irradiation. This irradiation resulted in the destruction of a perfect long range order ( $\text{DO}_3$  type) in a previously annealed alloy and of a less perfect long range order (B2 type) in a previously quenched alloy. Both the ordered and disordered specimens come to some quasiequilibrium condition at a fluence of about  $1.5 \times 10^{19} \text{ n/cm}^2$ . Irradiation in a high neutron flux does not create profound structural changes. The state formed is metastable, thus, slight heating of the specimen resulted in a partial recovery of the state which existed in the alloy before irradiation.

Betts [19] made electrical resistivity measurements of ordered, disordered, and intermediate states of  $\text{Fe}_3\text{Al}$  while being irradiated by neutrons. All specimens were irradiated at a temperature of about  $35^\circ\text{C}$ . Both the ordered and near ordered specimens increased in resistivity indicating disordering whereas the disordered and near disordered specimens decreased in resistivity due to ordering. An equilibrium condition was estimated at  $130 - 135 \text{ } \mu\text{ohm-cm}$  resistivity at a fluence of  $1.02 \times 10^{20} \text{ n/cm}^2$ . This was noted to be the resistivity that would remain constant during irradiation since the ordering and disordering effects of neutron irradiation would be in equilibrium.

Toma [20] investigated the ordering process from the B2 to the  $DO_3$  state and studied the fast neutron irradiation effects on the ordered superlattice. The specimen temperatures ranged from 100 to 300°C. The fast neutron flux was  $5.34 \times 10^9$  n/cm<sup>2</sup>-sec. Ordered specimens showed an advancement toward disorder and the disordered specimens indicated an advancement toward order. At a temperature of 300°C, the resistivities of both ordered and disordered samples tended to become constant as the fluence reached  $1.92 \times 10^{14}$  n/cm<sup>2</sup>. He found that this temperature was sufficient to cause an equilibrium between the ordering and disordering processes. During the determination of long range order parameters, he noted that the point defects produced during irradiation were annealed as the specimens were cooled from an elevated temperature to room temperature.

Artsishevskii and Selisskii [21] studied neutron irradiation effects in annealed, quenched, and work hardened specimens. The effects in the annealed and quenched alloys were similar to those reported by other authors. The work hardened alloy exhibited an increase in electrical resistivity at low temperatures and a decrease at high temperatures caused by neutron damage. It was suggested that disordering occurs at low temperatures and ordering takes place during recovery or recrystallization at high temperatures.

Artsishevskii, Vasil'ev, Kosheliaev, and Selisskii [22] studied the effect of deuteron bombardment on the electrical resistivity of  $Fe_3Al$ . The bombardment was carried out with a beam of deuterons of energy 4 MeV from a cyclotron. Thickness of the samples ranged from 20 - 30 microns to ensure interaction between the incident particles



and the lattice atoms throughout the whole volume of the sample. The ordered specimen was obtained by cooling at a rate of 25°/hr over the temperature range 550-250°C. The disordered specimen was achieved by rapid quenching from 850°C. In both the ordered and disordered irradiated samples, the change in resistivity were nearly identical. This seems to support the hypothesis of an intermediate degree of order being achieved due to bombardment. The change in the electrical resistivity due to bombardment may be connected with the formation of specific radiation damage, with change in the degree of order of the alloy, and with change in the Debye characteristic temperature.

#### E. RADIATION DAMAGE COMPUTER STUDIES INCLUDING $\text{Fe}_3\text{Al}$

In recent years there have been many investigations in the field of radiation damage utilizing the computer to simulate the various events which may occur due to radiation bombardment.

Gibson, Goland, Milgram, and Vineyard [23] studied the dynamics of radiation damage in the face centered cubic lattice of copper. The damage events were studied at low and moderate energies (up to 400 eV). In their model, no assumptions were required concerning what geometrical form the damaged configuration would take. A wide variety of initial conditions representing both static and dynamic events were used. For the static calculations the positions of the atoms in the defect were estimated and these coordinates were given to the computer generated crystallite atoms. The dynamic motion of these atoms was followed until a stable, or equilibrium, configuration was attained. A rather large lattice of atoms (about 500 to 1000) was considered. The atoms interact with two-body, central repulsive forces, and with the

stability of the lattice maintained by supplying additional forces to the surface atoms to simulate the binding effect of the crystallite being imbedded in a very large crystal lattice.

The results of this investigation provided evidence to support certain mechanisms that had been presented to explain radiation damage phenomena and evidence to disprove others. Damage at low energies consisted of vacancies and interstitials. Stability studies indicated that the interstitials reside in a split configuration in which it shares a lattice site with another atom. This configuration was originally proposed by Huntington and Seitz [24]. The character of the damage events are influenced by the regular arrangement of the lattice atoms. Certain directional chains focused at low energies and defocused at higher energies. Certain collision chains propagated with especially low loss of energy. A chain with energy above 25 or 30 eV carried matter, as well as energy, somewhat in the fashion of the "dynamic crowdion" which produces an interstitial near its end. In no case was this crowdion found to be stable. The decay rate of this defect, however, was rather slow and the authors felt that a slight change in the interatomic potential might make it stable. This "dynamic crowdion" action produced interstitials at a distance from the primary knock-on leaving vacancies behind in fairly compact groups. Another experimental result of the collision chains was the production of many more replacements than displacements. In alloys of nearly identical mass this would produce more disordered atoms than displaced atoms. The stability and threshold measurements of interstitial-vacancy pair formation was analyzed. The threshold energy for producing a single pair was found to be very directional dependent.

Also, the interstitial-vacancy pairs were found to be somewhat unstable.

Erginsoy, Vineyard, and Englert [25] modified the version of the Gibson et al. program to represent the body centered cubic alpha iron lattice. Low energy events were extensively investigated. Much of the experimental results closely paralleled the information gained from the face centered cubic copper program. The key mechanism of displacement at these low primary knock-on energies is a dynamic replacement mechanism in which the knock-on replaces one of the lattice atoms in the crystal. This replacement causes an extended sequence of correlated replacements, and an interstitial is formed a few atomic distances from the vacancy. This sequence is probably the most important mechanism in separating the interstitial and the vacancy. The stable interstitial form was found to be a split configuration oriented along  $\langle 110 \rangle$ . Interstitial-vacancy pairs were unstable against recombination when they are closely packed. The threshold energy for displacement was highly directional dependent. The energy thresholds for the  $\langle 100 \rangle$ ,  $\langle 110 \rangle$ , and  $\langle 111 \rangle$  directions were 17 eV, 34 eV, and 38 eV, respectively. Actually, the lowest thresholds associated with each of the above directions occurred a few degrees off the axis. The thresholds exactly along the axes were significantly higher. At such directions the energy threshold is limited by replacements outside the sphere of third neighbors. Also, the knock-on may displace one neighbor and replace another creating a divacancy. Results have shown that this takes place very easily if the two crystal axes involved have a relatively small angle between them as in the case of the  $\langle 110 \rangle$  and the  $\langle 111 \rangle$  directions.

Vineyard [26] subsequently made a third modification to the program of Gibson et al. to incorporate the order-disorder concept represented by  $\text{Cu}_3\text{Al}$ . Though only a few computer runs were made, the disordering effect was apparent under all conditions.

Erginsoy, Vineyard, and Shimizu [27] investigated the dynamics of radiation damage in a body centered cubic alpha iron lattice at energies up to 1.5 KeV. A primary knock-on with energy,  $E = 100$  eV, created an average 1.37 interstitial-vacancy pairs and for higher energies, the number of pairs increased as approximately,  $E/2E_d$ , where  $E_d$  was 50-55 eV. At energies around 100 eV, calculations on the eventual outcome of a single collision must allow for "many-body" aspects of the process to give even a fair approximation. Thus, this process must take into account the other atoms of the lattice as well as interactions between neighboring atoms. At all energies considered, damage consisted of vacancies and interstitials. Channeling did not appear to have any significance at low and intermediate energies. Channeling effects along  $\langle 100 \rangle$  and  $\langle 111 \rangle$  directions were significant when an iron atom of energy 1 KeV was introduced into the lattice from the outside. The rate of energy loss increased rapidly as the trajectory is displaced from the channel axis. Also, the change of energy with respect to time was found to be approximately constant, thus, the range of the channeled atom was approximately proportional to  $E_0^{3/2}$  where  $E_0$  is the initial energy.

Jackson, Leighly, and Edwards [28] used this same computer program to investigate radiation damage in  $\text{Fe}_3\text{Al}$  at low and intermediate energies. In all cases, the final damaged state consisted of vacancy-interstitial pairs. The distance of separation between these pairs

was a function of both energy and the direction of the primary knock-on. Again, the interstitial resided in a split configuration oriented in the  $\langle 110 \rangle$  direction. Also, as before, the threshold energies for displacement was found to be very directional dependent. The energy thresholds for the  $\langle 100 \rangle$  and  $\langle 110 \rangle$  directions are 22 eV, and 44 eV, respectively. The threshold for the  $\langle 111 \rangle$  direction was not determined due to its complex behavior. Replacement chains were found to be prevalent in the  $\langle 100 \rangle$  and  $\langle 110 \rangle$  directions. Focusing was observed in  $\langle 100 \rangle$  and  $\langle 111 \rangle$  directions and served as the primary mechanism for the dissipation of energy from the collision chain. Several events were greatly influenced by the presence of the aluminum atoms in the crystal lattice. The smaller mass of the aluminum atom present in the  $\langle 111 \rangle$  directional chain impeded the progress of the replacement chain. Defocusing events in the  $\langle 100 \rangle$  and  $\langle 111 \rangle$  directions were enhanced by the aluminum atom's low mass and high mobility. Disordering, prevalent in the defocusing chains, occurred from the general mixing of the lattice atoms along the chain and especially in a "plasticity spike" region near the end of the chain.

Jenkins [29] utilized Evaluated Nuclear Data File (ENDF/B) information to predict the primary recoil atom spectra of several elements in different reactor neutron spectra. The elements studied were nickel, niobium, and iron. Also generated were damage cross sections and optimum cutoff energies for use in comparing displacement damage in varying reactor spectra. No further details or method of calculation will be explained here since this program is similar to the one used by this study. Further details may be found in the following section on experimental procedure.

Doran [30-32] has investigated different models describing radiation damage in iron, chromium, nickel, stainless steel, and tantalum. Also described were different models used in simulating the production and short term behavior of defects due to fast ion bombardment. The energy dependent displacement cross section, generated for stainless steel, was based on the theory of slowing down of energetic atoms in solids due to Lindhard, et al. [33] rather than the Kinchin-Pease model for displacement efficiency per knock-on atom. In general,

$$D(E) = \sigma(E) \int_{T_{\min}}^{T_{\max}} K(E,T) \nu_L(T) dT \quad (9)$$

where

$D(E)$  = the energy dependent displacement cross section.

$\sigma(E)$  = the energy dependent scattering cross section.

$K(E,T)$  = the probability that a neutron of energy  $E$  transfers energy  $T$  to the knock-on atom.

$\nu_L(T)$  = the total number of displacements produced by a knock-on atom of energy  $T$  and is based on the Lindhard theory.

Knock-on atoms produced by fast neutrons are sufficiently energetic that appreciable energy is lost to electrons. The Lindhard model is a more realistic treatment of such ionization losses. The Kinchin-Pease model accounts for these losses only by designating a threshold energy above which all energy loss is by ionization (no displacements) and below which all energy loss results in displacements. The total number of displacements per knock-on atom based on the theory of Lindhard was taken to be

$$v_L(T) = \frac{L(\epsilon) T}{\epsilon 2E_d} \quad (10)$$

where

$$\epsilon = A_L T$$

$L(\epsilon)$  = a function which is kinetic energy in dimensionless form that is transferred to the atoms of a cascade initiated by a knock-on atom having initial dimensionless energy.

$L(\epsilon)/\epsilon$  = the fraction of knock-on atom energy available to cause displacements. The remainder is lost in electronic excitation.

$T$  = the kinetic energy of the knock-on atom in the laboratory system.

$E_d$  = the effective displacement energy.

$$A_L = \frac{0.8853 A_2}{(27.2)Z_1 Z_2 (Z_1^{2/3} + Z_2^{2/3})^{1/2} (A_1 + A_2)} \text{ eV}^{-1} \quad (11)$$

$A_1$  = the atomic weight of the moving particle.

$Z_1$  = the atomic number of the moving particle.

$A_2$  = the atomic weight of the lattice atoms.

$Z_2$  = the atomic number of the lattice atoms.

The expression for  $L(\epsilon)$  due to the work of Robinson [34] was used for convenience:

$$L(\epsilon) = \epsilon [1 + K_L g(\epsilon)]^{-1} \quad (12)$$

$$g(\epsilon) = \epsilon + 0.40244 \epsilon^{3/4} + 3.4008 \epsilon^{1/6} \quad (13)$$

From the theory of Lindhard

$$K_L = \frac{(0.0793) Z_1^{2/3} Z_2^{1/2} (A_1 + A_2)^{3/2}}{(Z_1^{2/3} + Z_2^{2/3})^{3/4} A_1^{3/2} A_2^{1/2}} \quad (14)$$

ENDF/B data was the source of information concerning anisotropic elastic and isotropic inelastic neutron scattering along with contributions from  $(n,\gamma)$  recoils and  $(n,2n)$  reactions. The major uncertainty in the study, aside from the question of the correctness of the program model, was in the low energy scattering cross sections and the energy dependence of the anisotropy at high energies which were obtained from the ENDF/B data.



### III. COMPUTATIONAL PROCEDURE

#### A. INTRODUCTION

The computer code RICE [1] was furnished by Oak Ridge National Laboratories. This code served as a body for SAKI. Also furnished were the ENDF/B II cross section libraries used by the code as well as GAM-II energy boundaries, damage cross sections of iron, and two neutron spectra for code input data. The two neutron spectra supplied are the unmodified fission neutron source spectrum and an HFIR spectra, which is a light water moderated, enriched uranium neutron spectrum. (See figure 5.)

The equations used by the code are now described. The symbols used are the same as the ones used in references [1] and [29].

#### B. CALCULATION OF THE ENERGY TRANSFER KERNEL

The energy transfer kernel,  $\sigma_s(E)K(E,T)$  is derived basically from the ENDF/B II cross section libraries.  $\sigma_s$  is the scattering cross section and  $K(E,T)$  describes the probability that a neutron scattering at energy  $E$  will transfer energy  $T$  to the target atom.

The elastic scattering cross sections are used with energy dependent Legendre coefficients to give the elastic-scattering energy transfer to the system. The Legendre coefficients are derived from Legendre expansions of the scattered-neutron angular distributions in the center-of-mass system. The energy,  $T$ , transferred to the target atom from a neutron of energy,  $E$ , is given as

$$T = \frac{(1-a)E}{2} (1-\cos\phi) \quad (15)$$

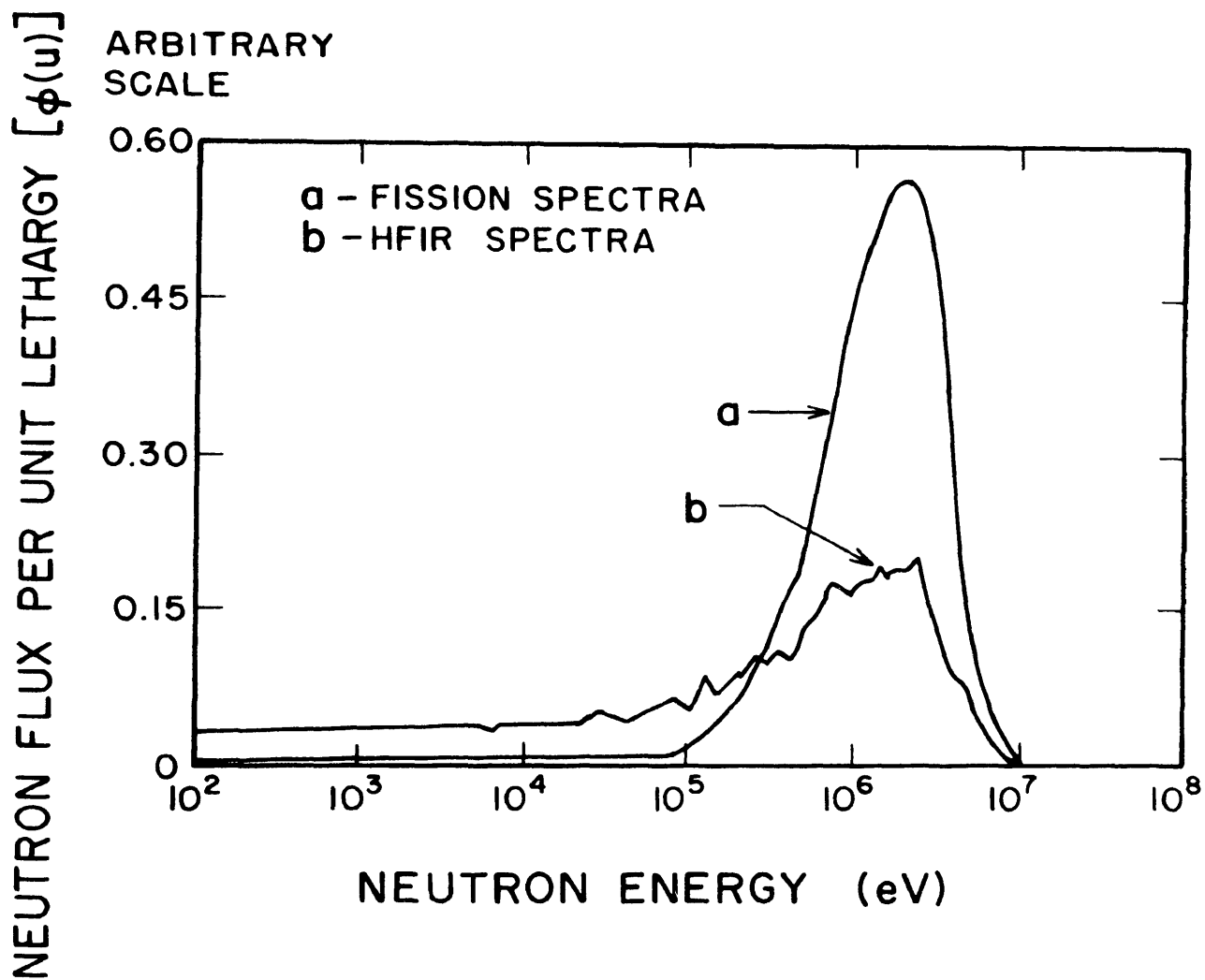


Figure 5. Two Representative Neutron Spectra Used in SAKI Calculations. Data is normalized to  $1 \text{ n/cm}^2\text{-sec}$  above  $1.86 \text{ eV}$ .

where

$$a = \left( \frac{M-m}{M+m} \right)^2$$

$M$  = the mass of the target atom

$m$  = neutron mass

$\phi$  = angle of scatter in the center-of-mass system

The scattered-neutron angular distributions are given in the form

$$\sigma_S(E, \cos\phi) = \sigma_S(E) \sum_{\ell} \frac{2\ell+1}{2} f_{\ell}(E) P_{\ell}(\cos\phi) \quad (16)$$

Subsequently, the elastic-scattering energy transfer kernel becomes

$$\sigma_S^{el}(E) k^{el}(E, T) = \sigma_S^{el}(E) \sum_{\ell} \frac{2\ell+1}{(1-a)E} f_{\ell}(E) P_{\ell} \left[ 1 - \frac{2T}{(1-a)E} \right] \quad (17)$$

The inelastic-scattering energy transfer kernel is derived from two components: the component from resolved resonance levels and the component from unresolved resonance levels. In addition to total inelastic cross sections  $\sigma_S^{in}(E)$ , energies of resolved excited levels of the target nucleus are given, together with the energy dependent fractions of the cross section which contribute to specific level excitations. For example, the inelastic-scattering cross section, which results in the excitation of the  $k$ -th level of the target nucleus to energy  $Q_k$ , is given by the expression  $\sigma_S^{in}(E) P_k(E)$  where  $P_k(E)$  is the fraction of the cross section contributing to the  $k$ -th level excitation. The contribution of the unresolved levels to the inelastic-scattering process is also given as a fraction of the total cross section,  $P_k(E)$ , and the scattered neutrons are assumed to be emitted from the compound nucleus with an energy distribution in the center-of-mass system described by the evaporation model. The emitted neutron spectrum is taken to be

$$\frac{1}{\theta^2(E)} E_m \exp[-E_m/\theta(E)] \quad (18)$$

where

$\theta(E)$  = energy dependent nuclear temperature supplied by ENDF/B II libraries

$E_m$  = the emitted neutron energy

In this representation there are  $K-1$  resolved levels and

$$\sum_{k=1}^K P_k(E) = 1 \quad (19)$$

For the excitation of a resolved level with energy  $Q_k$ , the energy transferred to the target atom is

$$T_k = \frac{1-a}{2} \left\{ E - \cos\phi [E(E-Q_k/\mu_2)]^{1/2} \right\} - Q_k \mu_1 \quad (20)$$

where

$$\mu_1 = m/M+m$$

$$\mu_2 = M/M+m$$

The upper and lower limits are designated  $T^+$  and  $T^-$ , respectively. They are obtained by setting  $\cos\phi$  to equal +1 and -1, respectively.

Assuming isotropic emission in the center-of-mass system and summing over the contributions of all the resolved levels gives the expression for the energy transfer kernel due to resolved level excitation:

$$\sigma_S^{in}(E) \sum_{k=1}^K P_k(E) K_k^r(E,T) = \sigma_S^{in}(E) \sum_{k=1}^{K-1} \frac{P_k(E)}{T_k^+(E) - T_k^-(E)} \quad (21)$$

where  $K_k^r(E,T)$  is the kernel for the  $k$ -th resolved level. Also, the  $k$ -th term in the sum is non-zero only for the situation where  $T$  is between or equal to the upper and lower limits on  $T$ .

The unresolved level situation is somewhat more complicated so the evaporation model is needed. If the neutron enters with an energy  $E$  in the center-of-mass system then the probability that the energy transferred will lie in  $dT$  about  $T$  is

$$P(E, E_m, T) dT = dT / 4\mu_1 (EE_m)^{1/2} \quad (22)$$

Using equation 22 and the evaporation spectrum gives:

$$\sigma_s^{in}(E) P_K(E) K^{ur}(E, T) dT = \frac{1}{C} \frac{\sigma_s^{in}(E) P_K(E)}{4\mu_1 \sqrt{E}} \int_{E_m^-}^{E_m^+} (E_m)^{1/2} \exp[-E_m/\theta(E)] dE_m dT \quad (23)$$

where

$K^{ur}(E, T)$  = the energy transfer kernel for the unresolved levels

$$E_m^-(E, T) = \mu_2^2 E - 2\mu_1 \left(\frac{M}{m}\right)^{3/2} (ET)^{1/2} + \left(\frac{M}{m}\right) T$$

$$E_m^+(E) = \mu_2 (\mu_2 E - Q_{K-1})$$

$$C = \theta^2(E) \left\{ 1 - \left[ \frac{\mu_2^2 E - \mu_2 Q_{K-1}}{\theta(E)} + 1 \right] \exp\left[ \frac{-\mu_2^2 E - \mu_2 Q_{K-1}}{\theta(E)} \right] \right\}$$

Integration of equation 23 yields:

$$\begin{aligned} \sigma_s^{in}(E) P_K(E) K^{ur}(E, T) = & \frac{\sigma_s^{in}(E) P_K(E)}{4C\mu_1 (E)^{1/2}} \left\{ \theta(E) \left\{ (E_m^-)^{1/2} \exp[-E_m^-/\theta(E)] \right. \right. \\ & \left. \left. - (E_m^+)^{1/2} \exp[-E_m^+/\theta(E)] \right\} \right. \\ & \left. + \theta^{3/2}(E) \frac{\pi^{1/2}}{2} \left[ \operatorname{erf} \frac{(E_m^+)^{1/2}}{\theta(E)} - \operatorname{erf} \frac{(E_m^-)^{1/2}}{\theta(E)} \right] \right\} \quad (24) \end{aligned}$$

This is the equation for the energy transfer kernel due to inelastic scattering by unresolved levels.

The complete transfer kernel is taken to be

$$\begin{aligned} \sigma_S(E) K(E,T) = & \sigma_S^{el}(E) K^{el}(E,T) + \sigma_S^{in}(E) \sum_{k=1}^{K-1} P_k(E) K_k^r(E,T) \\ & + \sigma_S^{in}(E) P_K(E) K^{ur}(E,T) \end{aligned} \quad (25)$$

where the terms on the right hand side are defined by equations 17, 21, and 24, respectively. The complete transfer kernel also makes full use of all data on anisotropic elastic scattering and inelastic scattering given by the ENDF/B II data.

The incident-neutron-energy mesh supplied by Oak Ridge National Laboratories was that of the GAM-II [35] program. There are one-tenth lethargy intervals from 14.9 to 0.11 MeV and one-quarter lethargy intervals from 0.11 MeV to 0.414 eV. The energy recoil mesh was defined by taking two hundred equal lethargy intervals between 25 eV and the maximum possible recoil energy,  $(1-a) \times 14.9$  MeV. The elements of the transfer matrix were defined by weighing the transfer kernel with an assumed  $1/E$  neutron spectrum over each neutron-energy group. The group-averaged quantities were found to be insensitive to the weighing function in the high-energy range when a  $1/E$  weighting is inappropriate. Thus,

$$K_{ij} = \frac{\int_{T_i}^{T_{i+1}} \int_{E_j}^{E_{j+1}} \frac{1}{E} \sigma_S(E) K(E,T) dE dT}{\int_{E_j}^{E_{j+1}} \frac{1}{E} dE} \quad (26)$$

This defines the energy transfer kernel.

### C. PRIMARY RECOIL ATOM SPECTRA

The primary recoil atom spectra per unit collision given a certain type neutron spectra,  $\phi(E)$  is:

$$K(T) = \frac{\int_0^{\infty} \sigma_s(E) \phi(E) K(E,T) dE}{\int_0^{\infty} \sigma_s(E) \phi(E) dE} \quad (27)$$

and the fraction of recoils above energy  $T$  can be obtained in the form

$$\text{Fraction above } T = \frac{\int_T^{\infty} K(T) dT}{\int_0^{\infty} K(T) dT} \quad (28)$$

This information may be used to estimate the size distribution of displacement spikes and also in the calculation of void formations.

### D. DAMAGE CROSS SECTIONS AND ENERGY CUTOFFS

The damage cross section,  $D(E)$ , describes the number of displacements per atom per neutron incident with energy  $E$ .

$$D(E) = \sigma_s(E) \int_0^{\infty} K(E,T) \nu(T) dT \quad (29)$$

where  $\nu(T)$  represents the total number of displacements caused by a primary neutron with energy  $T$  and is generated from the Kinchin and Pease [2] model. The total number of displacements caused by a given neutron spectrum is given by the expression

$$\frac{\text{Displacements}}{\text{Unit Flux}} = \frac{\int D(E) \phi(E) dE}{\int \phi(E) dE} \quad (30)$$

Equivalent damage energy cutoff calculations are obtained from the equation

$$D_E = \frac{\int_0^{\infty} \int_0^{\infty} \phi(E) \sigma_s(E) K(E,T) v(T) dT dE}{\int_E^{\infty} \phi(E) dE} \quad (31)$$

where  $D_E$  is the number of displacements per unit flux above  $E$ . For many irradiated elements or alloys a certain value of  $E = E_L$  can be found for which the displacement damage per exposure unit is almost independent of the neutron spectrum. The optimum cutoff energy for a given element or alloy can be calculated by evaluating  $D_E$  for several different spectra and locating the energy at which the plots of  $D_E$  vs.  $E$  approach each other.

#### E. COMPOUND CALCULATIONS

The compound energy mesh primary recoil atom spectrum may be defined as

$$K_C(T) = \frac{1}{N_1 + N_2} \frac{\int_0^{\infty} \left[ \Sigma_S^1(E) K^1(E,T) + \Sigma_S^2(E) K^2(E,T) \right] \phi(E) dE}{\int_0^{\infty} \phi(E) dE} \quad (32)$$



where

$N_1$  = the atom density of element 1

$N_2$  = the atom density of element 2

$\Sigma_S^1$  = the macroscopic cross section for scatter for element 1

$\Sigma_S^2$  = the macroscopic cross section for scatter for element 2

The compound composite energy transfer kernel can be defined as

$$K_{ij}^c = \frac{1}{N_1 + N_2} \frac{\int_{T_i}^{T_{i+1}} \int_{E_j}^{E_{j+1}} \left[ \Sigma_S^1(E) K^1(E, T) + \Sigma_S^2(E) K^2(E, T) \right] \frac{1}{E} dE dT}{\int_{E_j}^{E_{j+1}} \frac{1}{E} dE} \quad (33)$$

Calculation of the atom densities for iron and aluminum are needed.

$$\Sigma_{Fe_3Al} = \frac{N_A \rho_{Fe_3Al}}{M_{Fe_3Al}} [At.\%Fe \cdot \sigma_{Fe} + At.\%Al \cdot \sigma_{Al}] \text{ cm}^{-1} \quad (34)$$

where

$N_A = 6.025 \times 10^{23}$  molecules per mole of  $Fe_3Al$

$M = 194.56$  grams per mole

$\rho = 6.84$  grams per cubic centimeter

At.%Fe = 0.75

At.%Al = 0.25

For the compound  $Fe_3Al$ , there are four atoms per molecule.

Subsequently,

$$\Sigma_{\text{Fe}_3\text{Al}} = [6.369 \times 10^{22} \sigma_{\text{Fe}} + 2.123 \times 10^{22} \sigma_{\text{Al}}] \text{ cm}^{-1}$$

therefore,

$$N_{\text{Fe}} = 6.369 \times 10^{22} \text{ atoms per cubic centimeter}$$

$$N_{\text{Al}} = 2.123 \times 10^{22} \text{ atoms per cubic centimeter}$$

Also, the averaged atomic weight is found from:

$$\left( A_{\text{Fe}_3\text{Al}} \right)^{1/2} = \frac{3A_{\text{Fe}} + A_{\text{Al}}}{3 \left( A_{\text{Fe}} \right)^{1/2} + \left( A_{\text{Al}} \right)^{1/2}} \quad (35)$$

The atomic weight was found to be equal to 49.624. The atomic number was found to be 22.75. These two values were used in calculation of damage cross sections.

The damage cross section calculation for the compound is evaluated from

$$D(E)_c = \frac{1}{N_1 + N_2} \int_0^{\infty} \left[ \Sigma_s^1(E) K^1(E,T) v^1(T) + \Sigma_s^2(E) K^2(E,T) v^2(T) \right] dT \quad (36)$$

where

$v^1(T)$  = the total number of displacements in element 1

$v^2(T)$  = the total number of displacements in element 2

#### IV. COMPUTATIONAL RESULTS

Using the computer program previously described, the  $\text{Fe}_3\text{Al}$  damage cross section, and the primary recoil atom spectra in selected reactor environments, have been investigated.

##### A. DAMAGE CROSS SECTION FOR $\text{Fe}_3\text{Al}$

The energy dependent total iron damage cross section and the inelastic cross section generated by SAKI, are shown in figure 6. The inelastic scattering contribution contains the effect of nineteen resolved levels which range from 0.846 to 4.116 MeV. Determination of the damage cross section is based on ENDF/B data using the Kinchin-Pease model [2] for displacement calculations. From 0.01 to 5 MeV there is a general increase in the damage cross section followed by a sharp decrease which is characteristic of the Kinchin-Pease model. The inelastic component contributes to the total cross section above 0.846 MeV. A rapid increase followed by a sharp decline is typical of the inelastic component.

The aluminum damage cross section with its inelastic component is shown in figure 7. Contributions of inelastic scattering contain the effect of thirty-four resolved levels ranging from 0.943 to 15.25 MeV. These damage cross sections are also based on ENDF/B data and the Kinchin-Pease model. From 0.028 to 0.175 MeV there is a general increase in the total cross section followed by a general leveling off and a moderate decline from 2.6 to 15 MeV. The inelastic component contribution begins at 0.843 MeV and increases moderately to 15 MeV.

The damage cross section of  $\text{Fe}_3\text{Al}$  was determined and is shown in figure 8 along with its inelastic component. In the energy range,

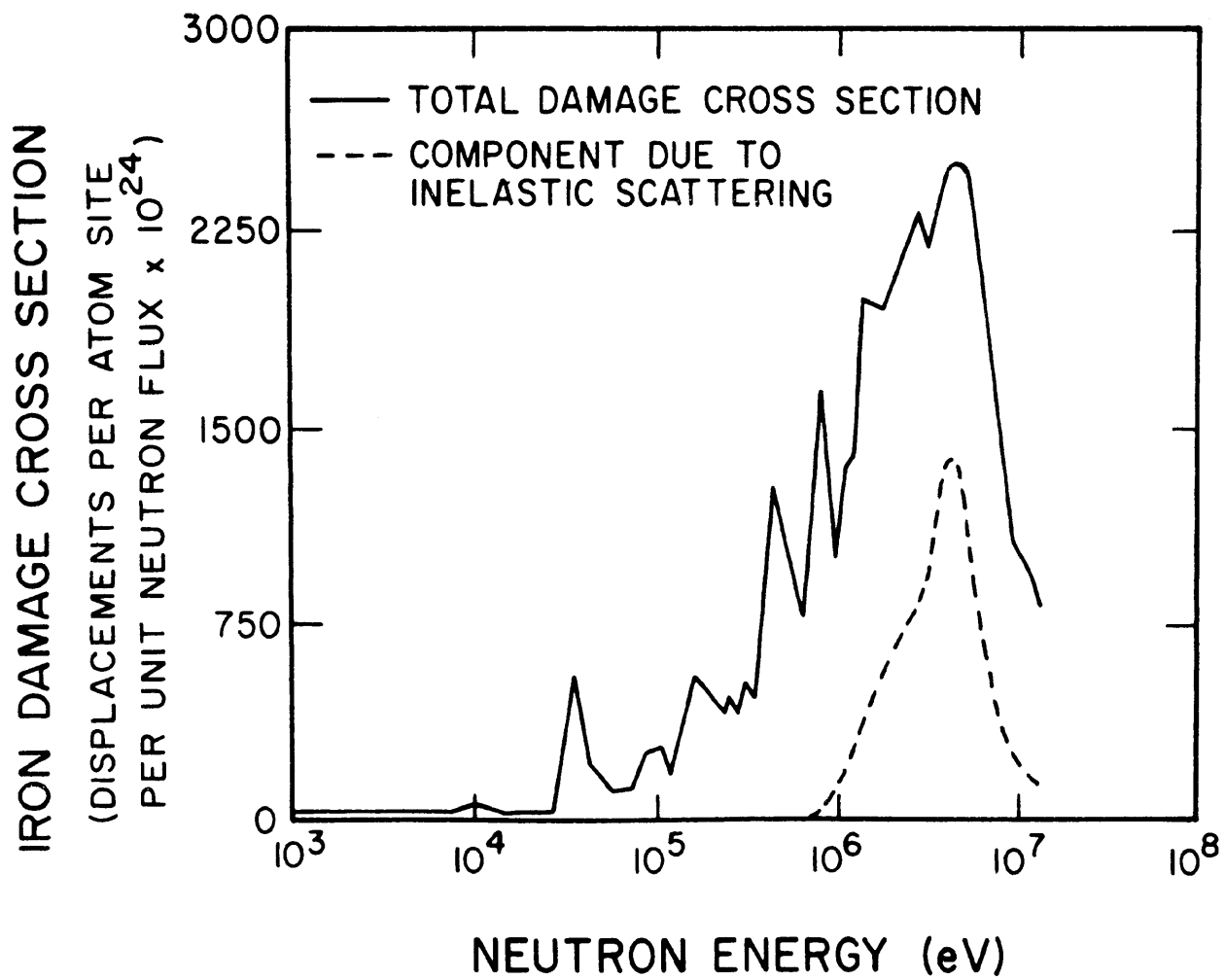


Figure 6. Iron Damage Cross Sections Calculated by SAKI.

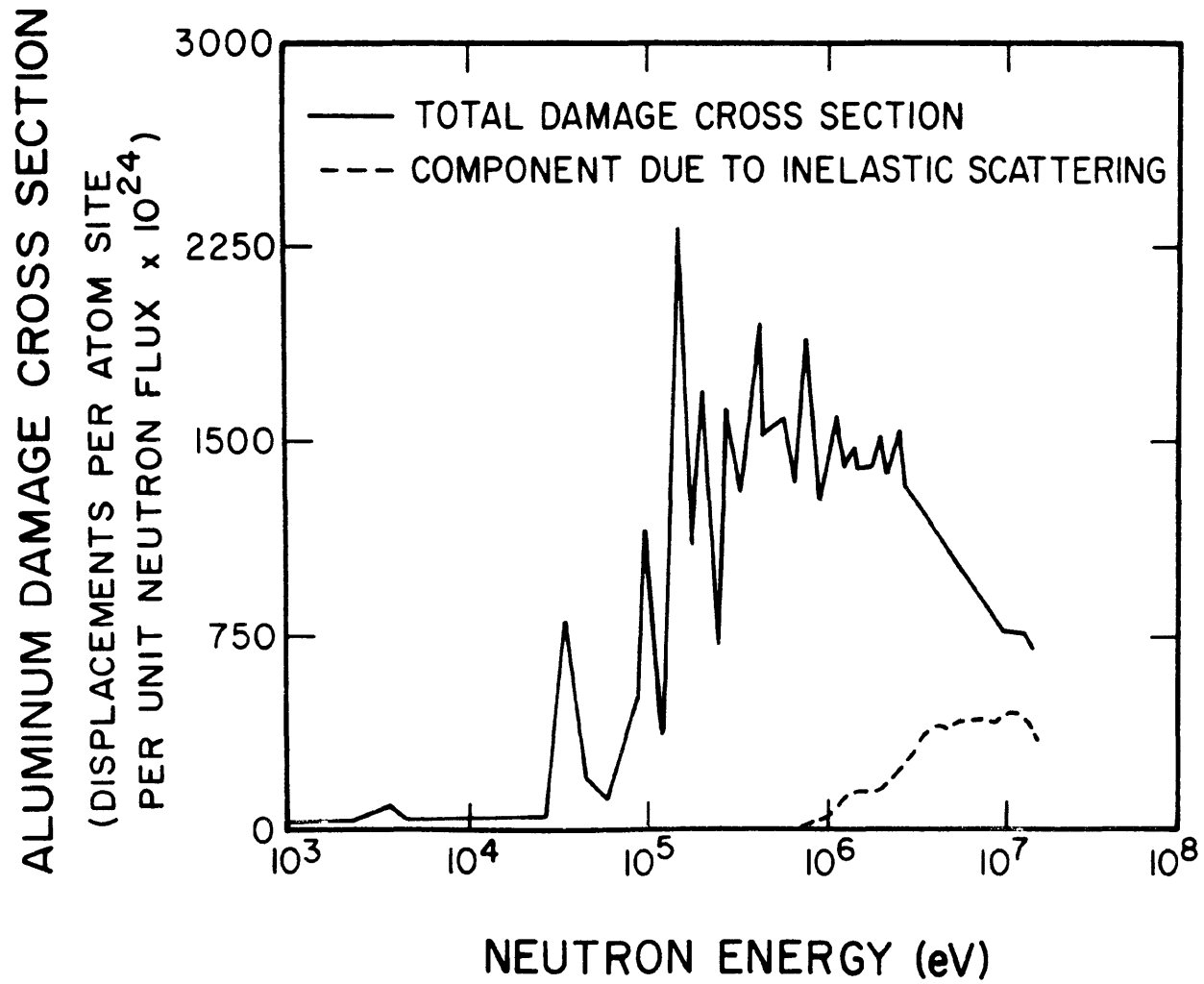


Figure 7. Aluminum Cross Sections Calculated by SAKI.

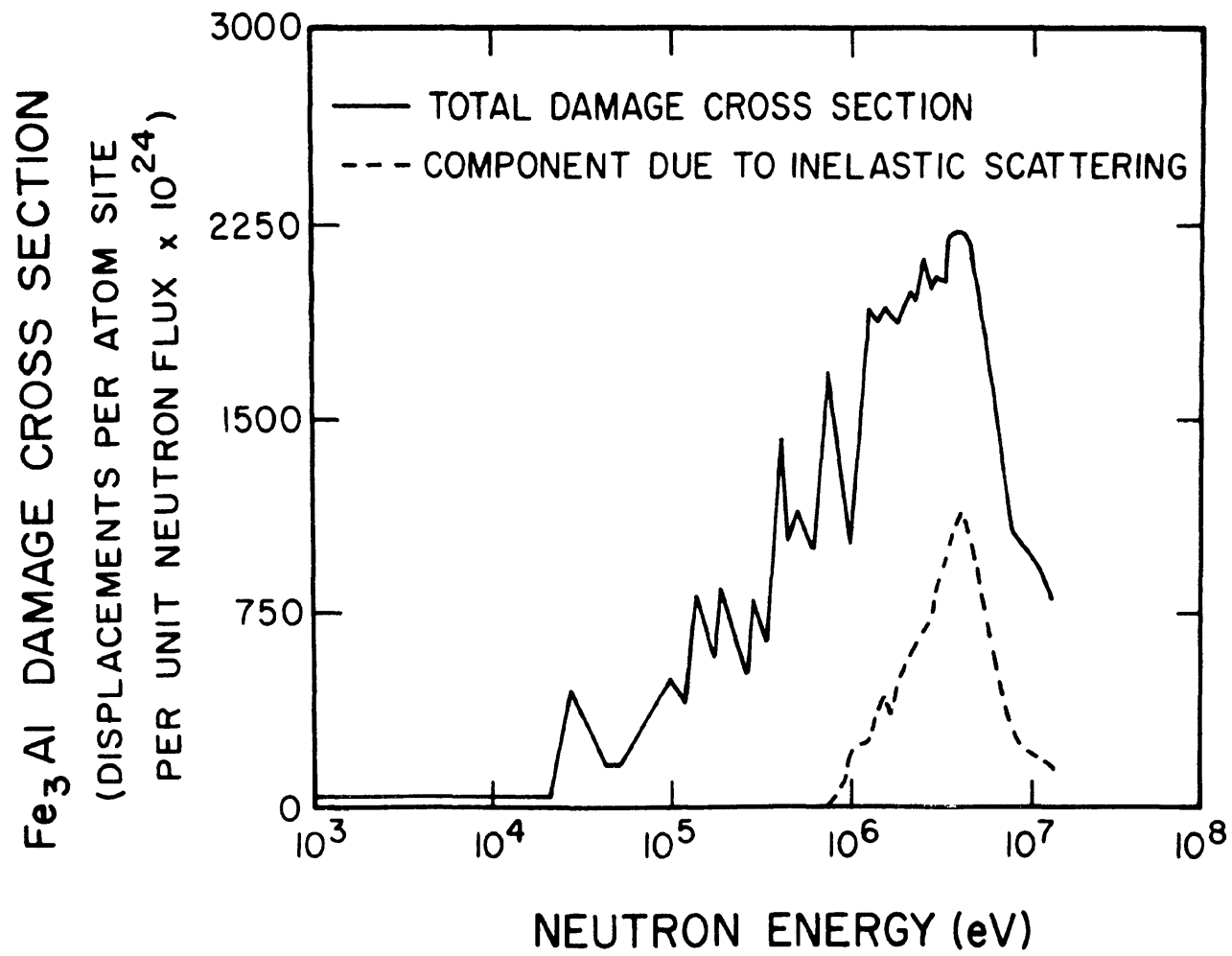


Figure 8. Damage Cross Sections of Fe<sub>3</sub>Al Calculated by SAKI.

0.02 to 5 MeV, there is a general increase in the total cross section followed by a rapid decrease to 15 MeV. The inelastic component contribution begins at 0.843 MeV and increases rapidly to 5 MeV followed by a sharp decline. At the lower energy levels, the  $\text{Fe}_3\text{Al}$  curve generally predicts a larger cross section than the pure iron curve, while above 1 MeV lower values are observed. It also exhibits more pronounced peaks as compared with the iron curve. This is the result of two effects: the presence of the lighter aluminum atoms in the alloy and the Kinchin-Pease model. Since the aluminum atom has about half the mass of the iron atom, it would be reasonable to assume that more displacements are expected. The aluminum curve shows a decline in cross section beginning at 2.6 MeV; the iron curve at about 5 MeV. These reductions are characteristic of the Kinchin-Pease model. Therefore, in the energy range from 2.6 to 15 MeV, the  $\text{Fe}_3\text{Al}$  damage cross section will be smaller than that of iron.

Tabulation of the damage cross sections of iron, aluminum, and  $\text{Fe}_3\text{Al}$  is found in Appendix B.

## B. PRIMARY RECOIL ATOM SPECTRA

This information is useful in estimating the size distribution of displacement spikes and can be used in calculations of void formations in irradiated materials.

Two neutron spectra were used to show the dependence of primary recoil energy distributions on the incident neutron distribution. They represent an unmoderated fission neutron source and a light water moderated, enriched uranium system (the HFIR reactor).

The resulting energy distributions are plotted as the fraction of recoils above the recoil atom energy as shown in figure 9. The effect

FRACTION OF RECOILS WITH ENERGY > T

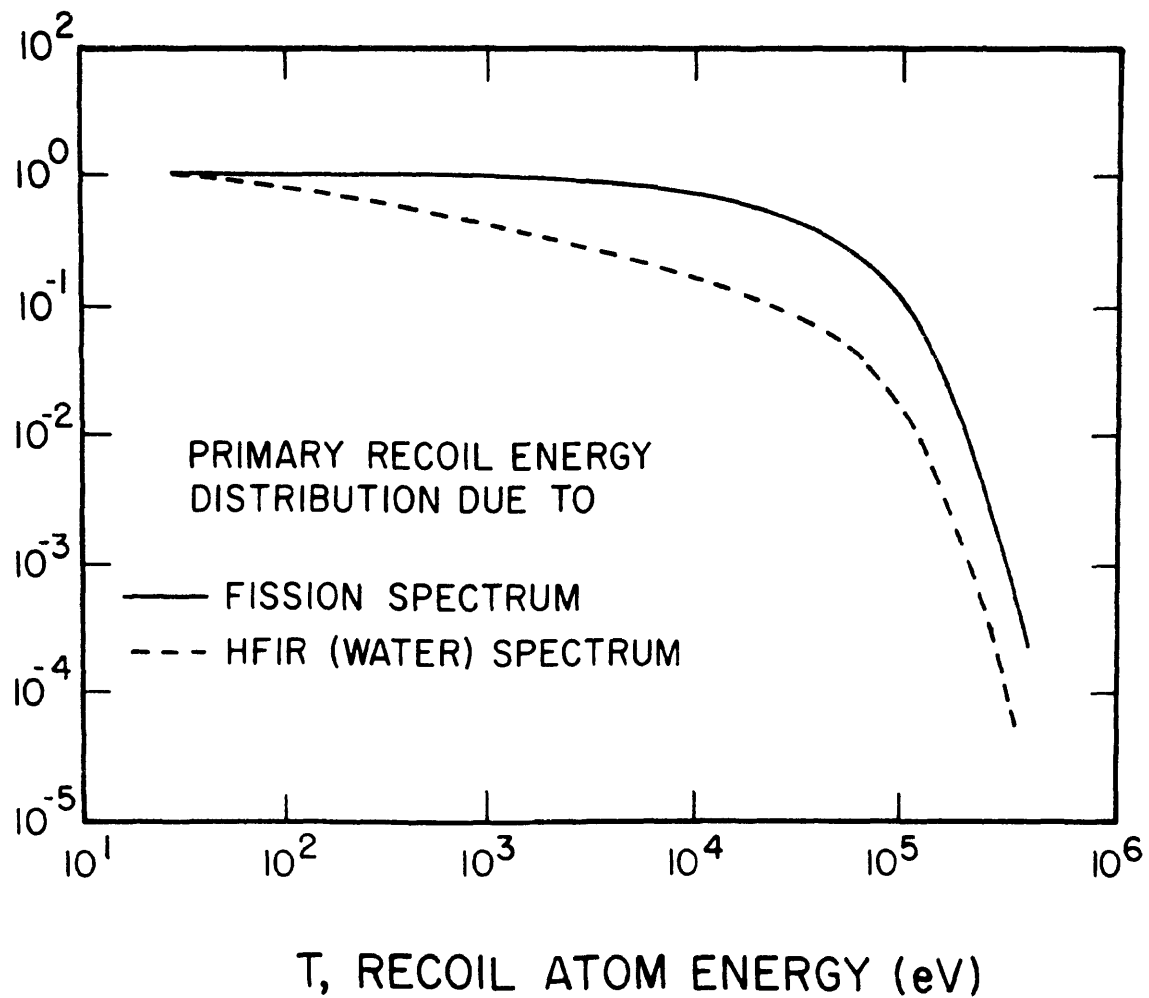


Figure 9. Energy Distribution of Fe<sub>3</sub>Al Recoil Atoms from Two Neutron Spectra.



of the incident neutron spectra is evident. For  $\text{Fe}_3\text{Al}$ , 90% of the primary recoils lie above 5 keV in a fission reactor spectra, while only 24% are produced above that energy by the HFIR spectra.

Tabulation of the primary recoil spectra for  $\text{Fe}_3\text{Al}$  is found in Appendix C.

## V. DISCUSSION OF RESULTS

The  $\text{Fe}_3\text{Al}$  damage cross section, shown in figure 8, describes the influence of elastic and inelastic scattering of iron and aluminum atoms under the influence of neutron radiation. It should be noted that the damage cross section gives only the number of primary collisions capable of producing damage and not the total number of atom displacements in a neutron system. For the latter it is necessary to take into account the additional displacements caused by secondary and tertiary collisions in a solid under the influence of a specific neutron spectra. The predominance of iron is readily apparent by comparing the shape of the iron and  $\text{Fe}_3\text{Al}$  curves. The additional resonance peaks in the  $\text{Fe}_3\text{Al}$  plot are due to the influence of the aluminum atoms in the alloy. These effects should be expected since  $\text{Fe}_3\text{Al}$  is composed of three times as many atoms of iron as aluminum. As stated before, the aluminum atom is about half the mass of the iron atom. It would be expected that for a given neutron energy a collision with an aluminum atom would produce a much larger number of displacements than a collision with an iron atom. Though this reasoning is not entirely correct since the lighter aluminum atoms will lose more energy by electronic excitation than iron atoms and in fact, limits the energy available for displacement. This effect, however, is less dominant in the  $\text{Fe}_3\text{Al}$  alloy than in a pure aluminum solid since the aluminum atom is surrounded by much heavier iron atoms. The aluminum atoms in  $\text{Fe}_3\text{Al}$  are more mobile and susceptible to displacement than the iron atoms. Because of this the  $\text{Fe}_3\text{Al}$  curve predicts a slightly larger cross

section than that of iron at low and intermediate energies. Only at high energies above 1 MeV does the  $\text{Fe}_3\text{Al}$  cross section show a smaller value than that of iron. Again, this is due predominantly to the effect of the Kinchin-Pease secondary displacement model used by SAKI.

The Kinchin-Pease model [2] is a bona fide description of the number of displacements produced by primary knock-on atoms of variable energies,  $T$ .

$$v(T) = \begin{cases} 0 & \text{for } 0 \leq T \leq E_d \\ 1 & \text{for } E_d \leq T \leq 2E_d \\ T/2E_d & \text{for } 2E_d \leq T \leq E_i \\ E_i/2E_d & \text{for } T \geq E_i \end{cases} \quad (37)$$

where  $E_d$  is the effective displacement energy, 25 eV. The main criticism [31] of this model is in the assumption of an upper PKO ionization energy threshold,  $E_i$ , above which all energy is lost in electronic excitation, and below which all energy is used either in producing displacements or generating lattice vibrations. This threshold for iron is 56 keV; aluminum is 27 keV. If a neutron with energy in excess of the PKO threshold hits the lattice atoms, not all of the energy received by the struck atoms is used in displacement production. In reality the sharp difference in mechanism of energy loss does not occur. A significant, decreasing fraction of the energy is used in producing displacement collisions at any primary energy above the threshold. The Kinchin-Pease model predicts a constant value of 1,120 displacements in iron produced by a primary displacement of energy above the PKO threshold; 540 atom displacements in aluminum.

Although this model is a convenient one, it is only approximate since the energy range of overlap of the ionization and collision loss processes may be appreciable. Thus, the main uncertainty in the correctness of the model lies mainly in the interpretation of events which lie above the PKO threshold energies for ionization in iron and aluminum.

The energy distributions of the primary recoil atoms of  $\text{Fe}_3\text{Al}$  in a fission and HFIR spectra are shown in figure 9. There is a profound effect on the fraction of recoils above the recoil atom energy due to the neutron environment. The neutrons emitted on fissioning of a  $\text{U}^{235}$  atom are distributed in energy from about 0.5 to 20 MeV with an average energy of 1.5 MeV. In the HFIR system, the energies of the neutrons are degraded as they pass through the light water moderator until they are thermalized. Thus, fewer fast neutrons are expected than in a fission spectra. In reactors the presence of thermal neutrons can lead to property changes due to artificial nuclear transmutations. However, in low cross section materials, such as iron and aluminum, this problem is dominant only after prolonged irradiation times. Interactions of fast neutrons with the lattice atoms produce several hundred vacancy-interstitial pairs due to the momentum which is transferred to the knock-on atom. As expected, the unmodified fission spectra indicates a more dynamic effect than that of the HFIR spectra. These energy distributions are of considerable importance to the total rate of damage in  $\text{Fe}_3\text{Al}$ . The difference in the curves is due entirely to the incident neutron spectra used in SAKI calculations and the information derived from the ENDF/B libraries.

This was the first extensive computer study of the damage cross section and primary recoil atom spectra of  $\text{Fe}_3\text{Al}$ , therefore, the results of this study could not be compared directly to similar work. However, there were a number of points in this study that could be compared with the work on iron damage cross sections by Jenkins [29], Sheely [35], and Doran [31].

A comparison of the iron damage cross sections determined by Jenkins and Sheely is shown in figure 10. The data was generated by techniques similar to those described in this study. The curves are in essential agreement, with the results of Jenkins predicting a higher displacement cross section for high energy neutrons and more fluctuations over the entire energy range. The difference in the curves are due to the additional detail available in the ENDF/B scattering cross sections. The inelastic scattering contribution calculated from ENDF/B data contains the effect of seven resolved levels and an unresolved contribution whereas Sheely's data attribute all the inelastic scattering to a single resolved level at 0.846 MeV.

Iron damage cross sections determined by Jenkins and Doran are shown in figure 11. The results of Doran predict a relatively lower damage cross section except at higher energies where a significant increase occurs. The difference in the curves are due to the two distinct models used for total displacements per primary knock-on atom. Jenkins used the Kinchin-Pease model [2] for the displacements produced per PKO and a displacement energy of 25 eV. Doran used the Lindhard model [33] based on the theory of energetic atoms in solids and is a more realistic treatment of ionization losses. He assumed a

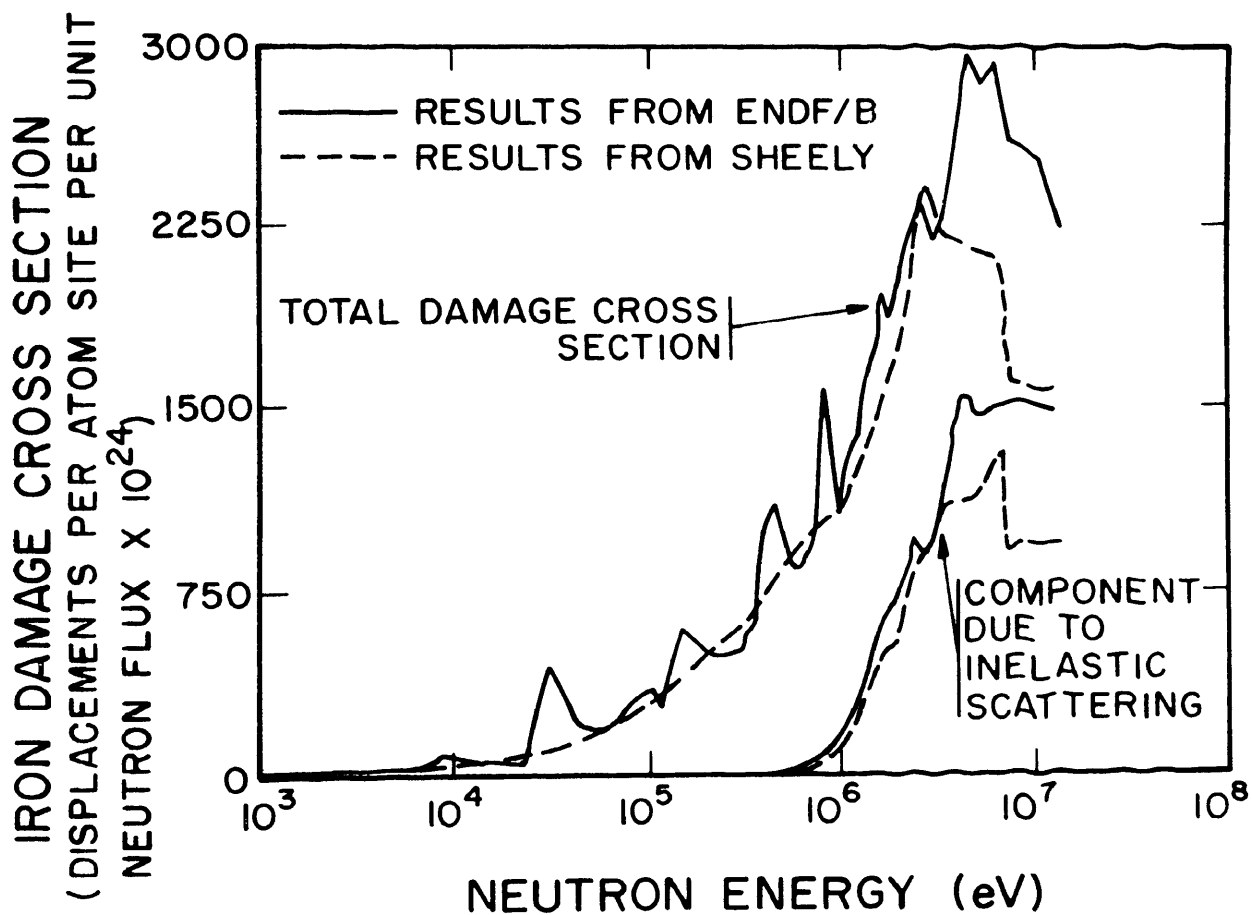


Figure 10. Comparison of Iron Damage Cross Sections from ENDF/B Data as Calculated by Jenkins [29] with Results Published by Sheely [35].

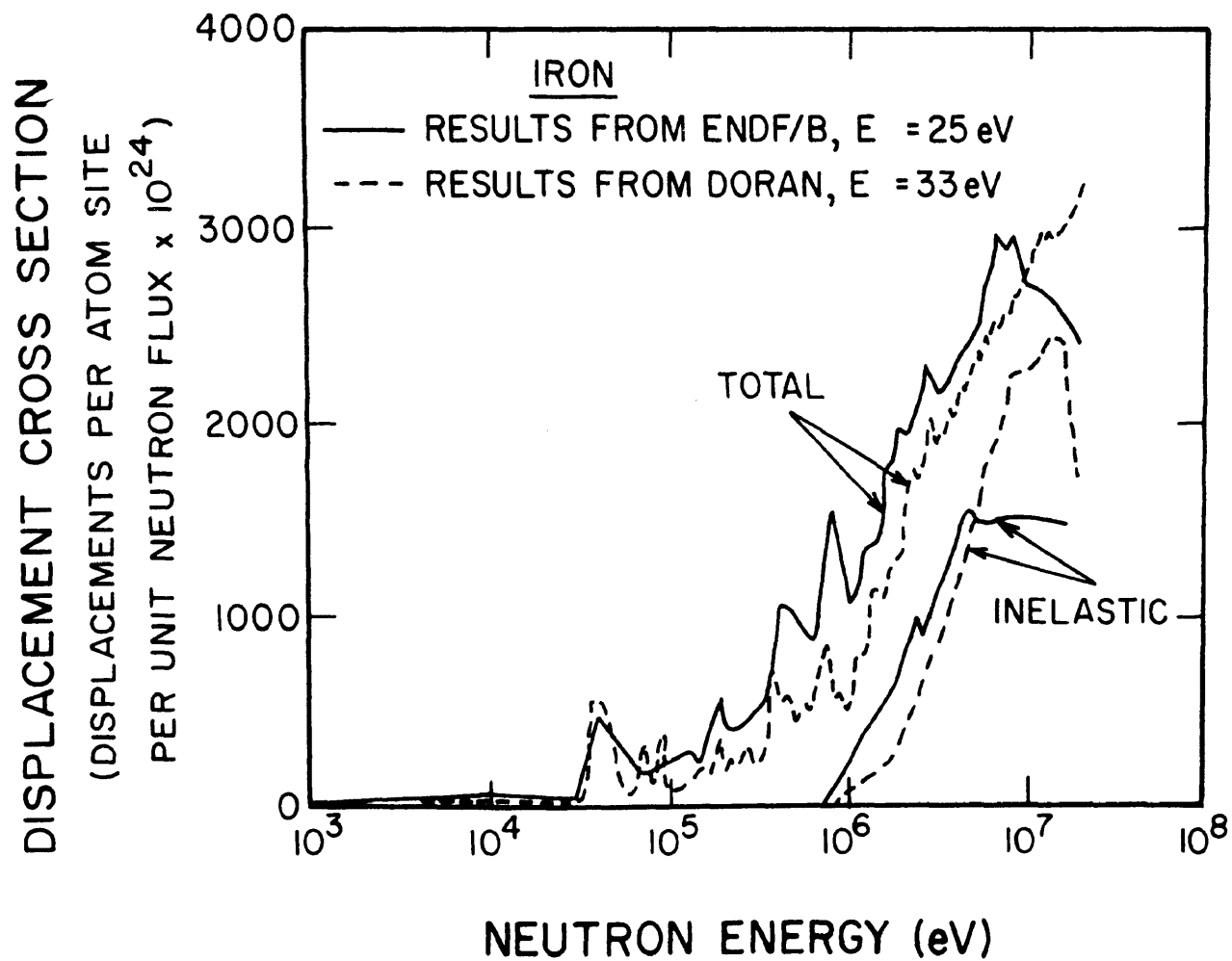


Figure 11. Comparison of Iron Damage Cross Sections from ENDF/B Data as Calculated by Jenkins [29] with Results Published by Doran [31].

displacement energy of 33 eV which is equivalent to 40 eV in the work of Jenkins. The relative decrease in Jenkins' cross section at high neutron energies is due to the Kinchin-Pease assumption of a primary knock-on ionization threshold energy of 56 keV above which all energy is dissipated in ionizing collisions that cause no displacements. In the Lindhard model a significant, although decreasing, fraction of the energy is lost in displacement producing collisions even at the highest primary knock-on energy of interest.

There is a general agreement between the iron damage cross section generated by SAKI and the data determined by Jenkins, except at neutron energies above 5 MeV. The difference is due to the additional resolved and unresolved resonance data above 5 MeV contained in Jenkins' ENDF/B Libraries.

SAKI assumes an overall effective displacement energy,  $E_d$ , of 25 eV throughout its computer run for all solids. Due to the configuration of nearest neighbors in the crystal lattice [28], the assumption of a discrete displacement energy threshold is a good approximation. Not only does  $E_d$  depend on the incident direction of the PKO but it may also vary from site to site within the lattice due to the mass difference of the alloying constituents.

A significant point to bring out is the inability of this investigation to predict the type and magnitude of certain damage mechanisms induced by radiation. Only an overall effect is presented describing the results due to elastic and inelastic scattering contributions. SAKI makes no distinction between the geometrical or sequential atomic arrangements in a given alloy system. Only the atomic percents of the



constituents of the alloy are considered here; this is analogous to the model of Doran [31]. It is therefore difficult to discern the effects, if any, that would be caused by the order-disorder phenomena.

The effect of high energy neutrons above 15 MeV cannot presently be stated with assurance, since the effect of other nuclear reactions, such as the (n,2n) reaction, is not known precisely. The (n,2n) reaction was neglected in this study. Energy thresholds in iron are 11-12 MeV but contributions were found to be minimal below 15 MeV [31]. Therefore, the omission of this contribution should not affect the results to any significant extent.

The tabulated values of the iron total damage cross section as determined by SAKI, Jenkins, and Doran are given in Appendix D.

## VI. CONCLUSIONS

The objectives of this study were to determine the energy dependent damage cross section and the primary recoil atom spectra of  $\text{Fe}_3\text{Al}$  in certain reactor environments.

An accurate description of the displacement process in  $\text{Fe}_3\text{Al}$  requires both the correct primary recoil atom spectra including the damage cross section and a valid secondary displacement model. The success of the Kinchin-Pease model [2], especially for low and intermediate energy neutrons, lends credence to the validity of the damage cross sections as well as the PKO spectra of  $\text{Fe}_3\text{Al}$ . This investigation removed a good bit of data uncertainty by correctly utilizing all available information contained in the ENDF/B library.

The energy dependent  $\text{Fe}_3\text{Al}$  damage cross section curve, as shown in figure 8, is successful in predicting the overall effect of neutron bombardment. The results presented are in reasonable agreement with the literature and certainly suggest the validity of this technique in calculating displacement cross sections for binary alloys.

As expected from the ratios of the cross sections, the iron atoms are the dominant influence in the alloy. Effects due to the aluminum atoms arise mainly from resonance peaks associated with the aluminum curve in figure 7. Contributions due to inelastic scattering has a very important additive effect at high incident neutron energies and is caused almost entirely by the iron atoms in the alloy.

Accurate representation of the primary recoil atom spectra of  $\text{Fe}_3\text{Al}$  required full utilization of ENDF/B neutron scattering data.

The PKO spectra is a means of measuring the relative merit of a reactor neutron environment. It is evident from the results of this study that the PKO spectra of  $\text{Fe}_3\text{Al}$  is a sensitive function of the two incident neutron spectra.

Valuable information has been derived from this study even though damage mechanisms due to radiation could not be determined. The exact mechanism by which displacements take place cannot be predicted by this computer program. It is felt, however, that there has been sufficient research in this area to establish primary displacement mechanisms in  $\text{Fe}_3\text{Al}$ . For example, see reference 28. Much more experimental work needs to be done to further our insight into damage processes in irradiated materials, such as  $\text{Fe}_3\text{Al}$ .

## VII. RECOMMENDATIONS

New data should be derived as supplemental information is available on the ENDF/B libraries. There is much uncertainty in the high neutron energy portion of the iron damage cross section curve which must be adequately described for a clearer understanding of displacement processes in  $\text{Fe}_3\text{Al}$ .

The choice of a good secondary displacement model must be made. As new investigations follow, this decision will be made clearer. The damage cross section of  $\text{Fe}_3\text{Al}$  should be calculated using the Lindhard model [33] to give a comparison between existing results.

Contributions due to  $(n,2n)$  reactions, though small, should be included in subsequent investigations as well as other possible reactions.

Experiments using controlled laboratory procedures may be performed to compare actual data to the predicted, as calculated by the computer. This is especially true when examining order-disorder alloys. The effect of ordering on the overall displacement process is an important part of the radiation damage explication.

## BIBLIOGRAPHY

1. Jenkins, J.D. "RICE: A Program to Calculate Primary Recoil Spectra from ENDF/B Data". U.S.A.E.C. Report ORNL-TM-2706. Oak Ridge National Laboratory, Oak Ridge, Tennessee (1970).
2. Kinchin, G.H. and R.S. Pease. Repts. Prog. Phys., 18, 1 (1955).
3. Johansson, C.H. and J.O. Linde. Ann. Physik, 78, 439 (1925).
4. Cohen, J.B. "The Order-Disorder Transformation". Phase Transformation. American Society for Metals, Metals Park, Ohio, pp. 561-624 (1970).
5. Bragg, W.L. and E.J. Williams. Proc. Roy. Soc., A151, 540 (1935).
6. Cowley, J.M. Phys. Rev., 77, 669 (1950); Phys. Rev., 120, 1648 (1960); Phys. Rev., 138, A1384 (1965).
7. Clapp, P.C. and S.C. Moss. Phys. Rev., 142, 418 (1966); Phys. Rev., 171, 754, 764 (1968).
8. Fosdick, L.D. Phys. Rev., 116, 565 (1959).
9. Guttman, L. Jour. Chem. Phys., 34, 1024 (1961).
10. Flinn, P.A. and G.M. McManus. Phys. Rev., A124, 54 (1961).
11. Bennet, W.D. "Some Effects of Order-Disorder in Iron-Aluminum Alloys". Journal of the Iron and Steel Institute, 171-172, 372 (1952).
12. Rauscher, G.P. "A Study of the Superlattice Transformations in Iron-Aluminum Alloys". Thesis, University of Denver, 71 pages (1962).
13. Leamy, H.J., E.D. Gibson, and F.X. Kayser. "The Elastic Stiffness Coefficients of Iron-Aluminum Alloys-I. Experimental Results and Thermodynamic Analysis". Acta Met., 15, 12, 1827-1838 (1967).
14. Wert, J.J. and S.G. Cupschalk. "Deformation Studies of Superlattice Structures". U.S.A.E.C. Report ORO-3091-7. Vanderbilt University (1967).
15. Marchinkowski, M.J. and N. Brown. "Direct Observation of Anti-phase Boundaries in the Fe<sub>3</sub>Al Superlattice". Jour. Appl. Phys., 33, 2, 537-552 (1962).

16. Krivogiaz, M.A. and A.A. Smirnov. The Theory of Order-Disorder in Alloys. American Elsevier Publishing Company, pp. 64-75 (1964).
17. Dautreppe, D. Studies of Radiation Effects in Solids. Vol. 3, pp. 97-119 (1969).
18. Saenko, G.P. Jour. Nucl. Mat., 11, 22 (1964).
19. Betts, B.A. "Fast Neutron Induced Resistivity Changes in Order-Disorder Fe<sub>3</sub>Al". M.S. Thesis, University of Missouri-Rolla, 87 pages (1968).
20. Toma, R.F. "Order-Disorder in Fe<sub>3</sub>Al at Various Temperatures Induced by Neutron Irradiation". M.S. Thesis, University of Missouri-Rolla, 90 pages (1969).
21. Artshishevskii, M.A. and Ia.P. Selisskii. Fiz. Metal. Metalloved, 11, 1, 20 (1961).
22. Artshishevskii, M.A., S.S. Vasil'ev, G.V. Kosheliaev, and Ia.P. Selisskii. Fiz. Metal. Metalloved, 7, 1, 53 (1959).
23. Gibson, J.B., A.N. Goland, M. Milgram, and G.H. Vineyard. Phys. Rev., 120, 4, 1229 (1960).
24. Huntington, H.B. and F. Seitz. Phys. Rev., 61, 315 (1942).
25. Erginsoy, C., G.H. Vineyard, and A. Englert. Phys. Rev. 133, 2A, A595 (1964).
26. Vineyard, G.H. Jour. Phys. Soc. Japan, 18, Supplement III, 144 (1963).
27. Erginsoy, C., G.H. Vineyard, and A. Shimizu. Phys. Rev., 139, 1A, A118 (1965).
28. Jackson, R.O., H.P. Leighly, Jr., D.R. Edwards. Phil. Mag., 25, 5, 1169 (1972).
29. Jenkins, J.D. Nucl. Sci. Eng., 41, 155 (1970).
30. Doran, D.G. "Some Implications of the Computer Simulation of Displacement Cascades in Radiation Modeling". Report HEDL-TME-71-181. Hanford Engineering Development Laboratory, Richland, Washington (1971).
31. Doran, D.G. "Displacement Cross Sections for Stainless Steel and Tantalum Based on a Lindhard Model". Nucl. Sci. Eng. (Accepted for Publication).

32. Doran, D.G. "Defect Production in Neutron Irradiations Inferred from Computer Experiments". Proceedings of the American Nuclear Society (June 1972).
33. Lindhard, J., V. Nielsen, M. Scharff, and P.V. Thomsen. Mat. Fys. Medd., 33, No. 14 (1963).
34. Robinson, M.T. Proceedings of Nuclear Fusion Reactors Conference, British Nuclear Energy Society, Culham Laboratory, Culham, England (1969).
35. Joanou, G.D. and J.S. Dudek. "GAM-II: A B<sub>3</sub> Code for the Calculation of Fast-Neutron Spectra and Associated Multigroup Constants". Report GA-4265, General Atomics (1963).

## VITA

The author was born on January 3, 1947 in Fulton, Missouri. He graduated from Fulton High School in May 1965.

He received his Bachelor of Science in Metallurgical Engineering-Nuclear Option in May 1970 from the University of Missouri-Rolla. He entered Graduate School in June 1970 at the University of Missouri-Rolla in the Department of Nuclear Engineering.



## APPENDIX A

## COMPUTER INPUT DATA

The order and description of the input data for SAKI, except for the compound calculations, conform closely to reference [1].

Execution of the section on compound calculations is initiated by assigning an integer value of twenty-five to ISEC. The next card indicates whether or not the compound total damage cross sections are desired to be punched. A non-zero value for IPOKE will punch the cross sections. A title or comment card was included in this section for the purpose of describing the alloy being considered. Atom densities are needed in the calculation of the compound's composite energy transfer kernel, PKO energy mesh, and damage cross sections. It should be noted that atom ratios may be used as input instead of atom densities. For example, there are three atoms of iron for every atom of aluminum in  $\text{Fe}_3\text{Al}$ . The input in this case would be 0.75 and 0.25 instead of the atom densities.

Two parameters used in Section Two of SAKI have been modified. A negative value for IIDAM indicates that there is one set of damage cross sections on logical 4 which is to be used in calculating optimum cutoff energies and PKO spectras. These cross sections were generated in Section One of SAKI and until now, could not be used in Section Two in the same computer run. Also, there is no plotting option in SAKI since no CRT plotter is available.

The SAKI input data follows.

1. GAM-II Energy Boundaries. EG(I), I=1,100. FORMAT(6E12.5).

1.491824+7	1.349859+7	1.220413+7	1.105171+7
1.000000+7	9.048374+6	8.187307+6	7.408182+6
6.703200+6	6.065306+6	5.488116+6	4.965853+6
4.493289+6	4.065696+6	3.678794+6	3.328711+6
3.011942+6	2.725318+6	2.465969+6	2.231301+6
2.018965+6	1.826835+6	1.652989+6	1.495686+6
1.353352+6	1.224564+6	1.108031+6	1.002588+6
9.071796+5	8.208501+5	7.427358+5	6.720552+5
6.081007+5	5.502322+5	4.978707+5	4.504921+5
4.076221+5	3.688317+5	3.337327+5	3.019738+5
2.732372+5	2.472353+5	2.237077+5	2.024191+5
1.831564+5	1.657267+5	1.499558+5	1.356856+5
1.227734+5	1.110900+5	8.651698+4	6.737949+4
5.247520+4	4.086772+4	8.182800+4	2.478800+4
1.930500+4	1.503400+4	1.170500+4	9.118088+3
7.101746+3	5.530845+3	4.307427+3	3.354627+3
2.612586+3	2.034684+3	1.584613+3	1.234098+3
9.611168+2	7.485185+2	5.829468+2	4.539994+2
3.535751+2	2.753646+2	2.144541+2	1.670170+2
1.300730+2	1.013009+2	7.889327+1	6.144214+1
4.785119+1	3.726654+1	2.902321+1	2.260330+1
1.760346+1	1.370959+1	1.067704+1	8.315290+0
6.475954+0	5.043478+0	3.927864+0	3.059024+0
2.382370+0	1.855392+0	1.444980+0	1.125352+0
8.764252-1	6.825606-1	5.315787-1	4.139939-1

2. Section One Execution for Iron. ISEC=1. FORMAT(14).

3. Control Parameters for Section One. FORMAT(15I4).

- a. MATNO=4124      Material identification on ENDF/B tape.
- b. IDTAP=0        Identification number of ENDF/B tape.
- c. MODE=2         Mode of ENDF/B data tape is BCD.
- d. IPIC=1         Calculate elastic, inelastic, and partial inelastic damage cross sections and energy exchange matrix.

- e. IRAS=0            Get smooth scattering cross sections from ENDF/B tape.
  - f. IWRT=1            Maximum printed output desired.
  - g. IPUNCH=0         No punched output desired.
  - h. IREC=1            Make the energy exchange matrix the first entry on logical 12.
  - i. IVERS=2          Version type of ENDF/B data.
4. Section One Execution for Aluminum. ISEC=1. FORMAT(I4).
5. Control Parameters for Section One. FORMAT(15I4).
- a. MATNO=4135
  - b. IDTAP=0
  - c. MODE=2
  - d. IPIC=1
  - e. IRAS=0
  - f. IWRT=1
  - g. IPUNCH=0
  - h. IREC=2
  - i. IVERS=2
6. Compound Calculation Execution for Iron and Aluminum. ISEC=25. FORMAT(I4).
7. Input for Compound Calculations.
- a. IPOKE=1            Punchout of compound total damage cross sections. FORMAT(I1).
  - b. Title or comment card. "Calculations on Fe<sub>3</sub>Al". FORMAT(20A4).
  - c. Atom Densities. FORMAT(2E20.10).
    - AN1=6.369            Atom density of iron in the compound x 10<sup>-22</sup>.
    - AN2=2.123            Atom density of aluminum in the compound x 10<sup>-22</sup>.

8. Section Two Execution. ISEC=2. FORMAT(I4).
9. Parameters for Section Two. FORMAT(10I4).
- a. NTAP=1            Process one set of energy exchange matrices from logical 12.
  - b. NDAM=-1         Process one set of damage cross sections from logical 4.
  - c. NFLUX=2         Read two sets of fluxes from cards.
  - d. IPUNCH=0        No punchout requested.
  - e. IPLOT=0         No plotting option available.
  - f. NREC=1          One matrix to be selected from logical 12.
10. Parameters used in Computing the Total Number of Displacements,  $\nu(T)$ . FORMAT(6E12.5).
- EXPRAM(1,1)=22.75
- EXPRAM(1,2)=49.624
11. Two Sets of Input Fluxes. First is the HFIR Spectra and the Second Set is the Fission Spectra.
- a. HFIR SPECTRA - Flux per Unit Lethargy. 99 Points.
- |             |             |             |             |
|-------------|-------------|-------------|-------------|
| 0.56110E-02 | 0.16310E-01 | 0.40830E-01 | 0.91490E-01 |
| 0.17990E 00 | 0.31710E 00 | 0.52810E 00 | 0.80830E 00 |
| 0.12010E 01 | 0.16600E 01 | 0.21550E 01 | 0.28370E 01 |
| 0.33030E 01 | 0.36310E 01 | 0.42760E 01 | 0.53730E 01 |
| 0.61160E 01 | 0.66870E 01 | 0.74790E 01 | 0.69330E 01 |
| 0.70410E 01 | 0.70330E 01 | 0.67120E 01 | 0.72980E 01 |
| 0.65620E 01 | 0.66110E 01 | 0.61320E 01 | 0.59280E 01 |
| 0.60320E 01 | 0.66050E 01 | 0.65260E 01 | 0.57520E 01 |
| 0.53190E 01 | 0.50120E 01 | 0.42120E 01 | 0.36440E 01 |
| 0.42520E 01 | 0.43530E 01 | 0.39200E 01 | 0.36570E 01 |
| 0.39390E 01 | 0.33120E 01 | 0.30080E 01 | 0.32200E 01 |
| 0.29160E 01 | 0.23180E 01 | 0.26000E 01 | 0.32430E 01 |
| 0.23910E 01 | 0.19160E 01 | 0.24980E 01 | 0.20250E 01 |
| 0.17960E 01 | 0.14890E 01 | 0.20000E 01 | 0.16680E 01 |

0.16090E 01	0.15710E 01	0.15410E 01	0.15190E 01
0.13750E 01	0.15800E 01	0.14880E 01	0.14770E 01
0.14700E 01	0.14610E 01	0.14510E 01	0.14410E 01
0.14310E 01	0.14200E 01	0.14100E 01	0.13990E 01
0.13870E 01	0.13680E 01	0.13610E 01	0.13500E 01
0.13410E 01	0.13300E 01	0.13190E 01	0.12710E 01
0.12720E 01	0.12190E 01	0.12300E 01	0.11650E 01
0.12020E 01	0.11360E 01	0.10980E 01	0.11250E 01
0.10920E 01	0.11150E 01	0.10920E 01	0.11010E 01
0.10870E 01	0.10860E 01	0.10520E 01	0.10150E 01
0.10050E 01	0.99690E 00	0.92360E 00	

b. FISSION SPECTRA - Flux per Unit Lethargy. 99 Points.

0.40580E-02	0.11260E-01	0.27460E-01	0.59380E-01
0.11720E 00	0.21440E 00	0.35990E 00	0.57310E 00
0.85040E 00	0.11960E 01	0.16100E 01	0.20690E 01
0.25520E 01	0.30370E 01	0.35330E 01	0.40040E 01
0.43750E 01	0.46570E 01	0.49560E 01	0.52970E 01
0.57850E 01	0.61510E 01	0.63460E 01	0.67440E 01
0.71900E 01	0.76470E 01	0.84450E 01	0.96490E 01
0.11360E 02	0.12030E 02	0.12120E 02	0.14530E 02
0.15950E 02	0.18400E 02	0.16860E 02	0.16410E 02
0.16140E 02	0.17160E 02	0.15940E 02	0.15870E 02
0.13800E 02	0.12930E 02	0.11730E 02	0.11820E 02
0.11270E 02	0.97060E 01	0.87290E 01	0.77740E 01
0.68560E 01	0.53600E 01	0.39120E 01	0.22720E 01
0.27510E 01	0.15820E 01	0.88120E 00	0.52210E 00
0.27650E 00	0.13090E 00	0.81940E-01	0.59490E-01
0.24690E-01	0.14200E-01	0.50890E-02	0.19520E-02
0.48440E-02	0.67110E-02	0.25970E-02	0.85550E-03
0.37030E-03	0.11000E-03	0.16320E-03	0.91670E-04
0.61750E-04	0.10210E-04	0.22230E-05	0.22920E-05
0.11590E-04	0.41580E-04	0.14670E-04	0.26080E-05
0.10820E-05	0.64950E-06	0.20080E-05	0.11870E-05
0.22520E-05	0.73480E-06	0.48210E-06	0.11760E-05

0.58280E-06	0.11000E-05	0.54350E-06	0.90300E-06
0.51310E-06	0.55420E-06	0.16880E-06	0.68940E-07
0.72760E-07	0.47430E-07	0.27150E-07	

12. End of Job Indicator. ISEC=0. FORMAT(I4).

## APPENDIX B

DAMAGE CROSS SECTIONS OF IRON, ALUMINUM, AND Fe<sub>3</sub>Al  
CALCULATED FROM SAKI

## A. Total Damage Cross Sections

Total Damage Cross Sections  
(displacements per atom/unit flux x 10<sup>24</sup>)

<u>Energy, MeV</u>	<u>Iron</u>	<u>Aluminum</u>	<u>Fe<sub>3</sub>Al</u>
14.208	854.92	731.37	824.08
12.851	912.03	759.90	874.00
11.627	980.80	765.70	927.03
10.525	1059.78	769.50	987.21
9.524	1153.51	772.27	1058.20
8.618	1251.26	810.93	1141.18
7.797	1422.65	860.55	1282.13
7.055	1633.25	908.02	1451.94
6.384	1880.75	973.61	1653.96
5.776	2143.40	1006.23	1859.11
5.227	2386.60	1054.50	2053.58
4.729	2577.25	1063.61	2198.84
4.279	2589.12	1115.79	2220.79
3.872	2534.48	1190.77	2198.55
3.504	2363.44	1234.54	2081.22
3.170	2375.39	1214.23	2085.10
2.868	2243.12	1297.06	2006.60
2.595	2340.08	1539.15	2139.85
2.348	2146.55	1293.50	1933.29

<u>Energy, MeV</u>	<u>Iron</u>	<u>Aluminum</u>	<u>Fe<sub>3</sub>Al</u>
2.125	2154.10	1493.26	1988.89
1.923	2031.64	1366.08	1865.25
1.740	1787.80	1374.61	1684.50
1.574	1912.15	1382.23	1779.67
1.424	1778.53	1424.24	1689.96
1.288	1932.12	1328.29	1781.17
1.166	1364.02	1682.41	1443.62
1.055	1325.28	1270.45	1311.57
0.955	1029.70	1225.80	1078.73
0.864	1070.16	1671.28	1220.45
0.782	1657.56	1894.57	1716.81
0.707	1371.09	1290.61	1350.97
0.640	778.80	1661.45	999.46
0.579	888.55	1542.04	1051.92
0.524	993.42	1570.65	1137.72
0.474	913.71	1503.58	1061.18
0.429	1263.05	1947.88	1434.26
0.388	1048.78	1284.26	1107.65
0.351	496.31	1246.99	683.98
0.317	584.38	1448.73	800.47
0.287	544.86	1657.15	822.93
0.260	422.33	742.76	502.43
0.235	496.97	1102.41	648.34
0.213	443.40	1734.83	766.26
0.193	745.53	1104.73	835.33



<u>Energy, MeV</u>	<u>Iron</u>	<u>Aluminum</u>	<u>Fe<sub>3</sub>Al</u>
0.174	378.99	1276.70	603.42
0.158	275.07	2297.16	780.59
0.143	573.93	1619.54	835.33
0.129	279.59	344.61	295.85
0.116	170.22	779.37	322.51
$9.88 \times 10^{-2}$	287.12	1151.71	503.27
$7.69 \times 10^{-2}$	375.87	469.04	399.16
$5.99 \times 10^{-2}$	171.21	149.14	165.69
$4.67 \times 10^{-2}$	167.09	229.69	182.74
$3.63 \times 10^{-2}$	210.52	797.75	357.33
$2.83 \times 10^{-2}$	615.28	49.89	473.94
$2.20 \times 10^{-2}$	11.10	21.67	13.74
$1.71 \times 10^{-2}$	23.99	24.43	24.10
$1.33 \times 10^{-2}$	29.12	24.42	27.95
$1.04 \times 10^{-2}$	36.72	19.20	32.34
$8.11 \times 10^{-3}$	88.31	15.78	70.18
$6.31 \times 10^{-3}$	39.02	24.58	35.41
$4.91 \times 10^{-3}$	19.27	10.27	17.02
$3.83 \times 10^{-3}$	18.35	7.85	15.72
$2.98 \times 10^{-3}$	13.78	6.20	11.89
$2.32 \times 10^{-3}$	11.88	4.89	10.13
$1.81 \times 10^{-3}$	10.14	3.82	8.56
$1.41 \times 10^{-3}$	8.55	2.97	7.15
$1.09 \times 10^{-3}$	7.06	2.31	5.87
$8.54 \times 10^{-4}$	5.60	1.79	4.65

<u>Energy, MeV</u>	<u>Iron</u>	<u>Aluminum</u>	<u>Fe<sub>3</sub>Al</u>
6.65 x 10 <sup>-4</sup>	4.55	1.39	3.76
5.18 x 10 <sup>-4</sup>	3.13	1.08	2.62
4.04 x 10 <sup>-4</sup>	1.10	0.84	1.03
3.14 x 10 <sup>-4</sup>	0.0	0.63	0.16
2.45 x 10 <sup>-4</sup>	0.0	0.39	0.09
1.91 x 10 <sup>-4</sup>	0.0	0.09	0.02
1.48 x 10 <sup>-4</sup>	0.0	0.0	0.0

#### B. Inelastic Damage Cross Sections

Inelastic Damage Cross Sections  
(displacements per atom per unit flux x 10<sup>24</sup>)

<u>Energy, MeV</u>	<u>Iron</u>	<u>Aluminum</u>	<u>Fe<sub>3</sub>Al</u>
14.208	125.84	363.88	185.35
12.851	134.80	401.51	201.48
11.627	149.70	426.01	218.77
10.525	165.07	432.67	231.97
9.524	202.92	426.10	258.71
8.618	279.31	427.18	316.28
7.797	399.92	433.23	408.25
7.055	559.73	435.23	528.61
6.384	756.44	433.82	675.79
5.776	983.70	428.99	845.02
5.227	1217.37	414.65	1016.69
4.729	1376.76	384.15	1112.86
4.279	1404.77	400.56	1153.72
3.872	1331.72	386.64	1095.45

<u>Energy, MeV</u>	<u>Iron</u>	<u>Aluminum</u>	<u>Fe<sub>3</sub>Al</u>
3.504	1145.95	340.33	944.55
3.170	1049.92	288.41	859.54
2.868	867.62	260.80	715.92
2.595	751.15	241.40	623.71
2.348	743.08	181.89	602.79
2.125	687.64	161.03	555.98
1.923	542.40	159.27	446.62
1.740	436.95	155.28	366.53
1.574	474.73	149.70	393.47
1.424	442.92	139.51	367.07
1.288	324.89	119.33	273.50
1.166	351.59	82.07	284.21
1.055	228.88	41.23	181.96
0.955	119.64	16.43	93.84
0.864	42.34	0.98	32.00
0.782	0.0	0.0	0.0

## APPENDIX C

ENERGY DISTRIBUTION OF Fe<sub>3</sub>Al RECOIL ATOMS FROM TWO NEUTRON SPECTRA

<u>T, Recoil Energy (eV)</u>	Fraction of Recoils with Energy > T	
	<u>HFIR Spectra</u>	<u>Fission Spectra</u>
0.2638 x 10 <sup>2</sup>	0.9994	0.9999
0.3457 x 10 <sup>2</sup>	0.9973	0.9997
0.4530 x 10 <sup>2</sup>	0.9908	0.9995
0.5937 x 10 <sup>2</sup>	0.9643	0.9991
0.7780 x 10 <sup>2</sup>	0.9185	0.9990
0.1019 x 10 <sup>3</sup>	0.8325	0.9989
0.1336 x 10 <sup>3</sup>	0.7583	0.9986
0.1751 x 10 <sup>3</sup>	0.6774	0.9983
0.2296 x 10 <sup>3</sup>	0.6609	0.9980
0.3010 x 10 <sup>3</sup>	0.5730	0.9974
0.3946 x 10 <sup>3</sup>	0.5497	0.9961
0.5173 x 10 <sup>3</sup>	0.4948	0.9950
0.6783 x 10 <sup>3</sup>	0.4563	0.9938
0.8894 x 10 <sup>3</sup>	0.4191	0.9926
0.1166 x 10 <sup>4</sup>	0.3812	0.9912
0.1529 x 10 <sup>4</sup>	0.3457	0.9880
0.2006 x 10 <sup>4</sup>	0.3037	0.9805
0.2630 x 10 <sup>4</sup>	0.2886	0.9557
0.3450 x 10 <sup>4</sup>	0.2642	0.9371
0.4526 x 10 <sup>4</sup>	0.2334	0.9125
0.5937 x 10 <sup>4</sup>	0.2221	0.8643

<u>T, Recoil Energy (eV)</u>	Fraction of Recoils with Energy > T	
	<u>HFIR Spectra</u>	<u>Fission Spectra</u>
0.7789 x 10 <sup>4</sup>	0.1890	0.8326
0.1021 x 10 <sup>5</sup>	0.1755	0.7954
0.1340 x 10 <sup>5</sup>	0.1448	0.7110
0.1759 x 10 <sup>5</sup>	0.1383	0.6602
0.2308 x 10 <sup>5</sup>	0.1025	0.5523
0.3029 x 10 <sup>5</sup>	0.0864	0.5044
0.3976 x 10 <sup>5</sup>	0.0700	0.4399
0.5218 x 10 <sup>5</sup>	0.0455	0.3623
0.6849 x 10 <sup>5</sup>	0.0381	0.2350
0.8991 x 10 <sup>5</sup>	0.0201	0.1452
0.1180 x 10 <sup>6</sup>	0.0074	0.0906
0.1549 x 10 <sup>6</sup>	0.0024	0.0265
0.2034 x 10 <sup>6</sup>	0.0008	0.0086
0.2671 x 10 <sup>6</sup>	0.0001	0.0022

## APPENDIX D

## IRON DAMAGE CROSS SECTIONS AS DETERMINED BY SAKI, JENKINS, AND DORAN

Total Damage Cross Sections for Iron  
(displacements per atom per unit neutron flux  $\times 10^{24}$ )

<u>Energy, MeV</u>	<u>SAKI</u>	<u>Jenkins</u>	<u>Doran</u>
14.208	854.92	2151.01	3370.76
12.851	912.03	2245.36	3138.16
11.627	980.80	2332.53	3011.40
10.525	1059.78	2430.52	2958.80
9.524	1153.51	2541.07	2898.55
8.618	1251.26	2575.88	2866.85
7.797	1422.65	2582.56	2885.82
7.055	1633.25	2630.41	2797.94
6.384	1880.75	2884.34	2671.78
5.776	2143.40	2971.85	2570.30
5.227	2386.60	2797.65	2513.63
4.729	2577.25	2874.88	2459.12
4.279	2589.12	2971.11	2379.08
3.872	2534.48	2746.00	2241.60
3.504	2363.44	2387.74	2078.39
3.170	2375.39	2297.58	2086.23
2.868	2243.12	2116.23	1929.55
2.595	2340.08	2333.24	1867.49
2.348	2146.55	2293.98	1762.76
2.125	2154.10	2128.36	1588.99
1.923	2031.64	1994.05	1528.61

<u>Energy, MeV</u>	<u>SAKI</u>	<u>Jenkins</u>	<u>Doran</u>
1.740	1787.80	1829.69	1240.32
1.574	1912.15	1995.42	1197.43
1.424	1778.53	1674.37	1146.98
1.288	1932.12	1702.27	1096.33
1.166	1364.02	1329.36	991.66
1.055	1325.28	1332.48	781.48
0.955	1029.70	975.10	747.16
0.864	1070.16	1099.82	670.53
0.782	1657.56	1597.34	769.19
0.707	1371.09	1251.37	743.12
0.640	778.80	860.42	576.50
0.579	888.55	799.59	502.45
0.524	993.42	856.30	524.30
0.474	913.71	993.72	537.48
0.429	1263.05	1100.47	632.13
0.388	1048.78	1031.35	648.68
0.351	496.31	561.32	363.37
0.317	584.38	578.39	383.87
0.287	544.86	466.96	278.10
0.260	422.33	459.94	281.59
0.235	496.97	467.81	299.33
0.213	443.40	445.12	260.07
0.193	745.53	495.10	393.55
0.174	378.99	512.35	257.06
0.158	275.07	544.74	251.02

<u>Energy, MeV</u>	<u>SAKI</u>	<u>Jenkins</u>	<u>Doran</u>
0.143	573.93	612.42	387.82
0.129	279.59	366.91	238.82
0.116	170.22	274.18	125.94
$9.88 \times 10^{-2}$	287.12	332.99	232.47
$7.69 \times 10^{-2}$	375.87	298.14	165.63
$5.99 \times 10^{-2}$	171.21	169.70	105.28
$4.67 \times 10^{-2}$	167.09	155.24	99.08
$3.63 \times 10^{-2}$	210.52	192.96	97.07
$2.83 \times 10^{-2}$	615.28	475.06	73.79
$2.20 \times 10^{-2}$	11.10	15.40	21.29
$1.71 \times 10^{-2}$	23.99	33.42	42.60
$1.33 \times 10^{-2}$	29.12	39.20	36.48
$1.04 \times 10^{-2}$	36.72	46.07	26.10
$8.11 \times 10^{-3}$	88.31	87.71	52.77
$6.31 \times 10^{-3}$	39.02	36.64	30.46
$4.91 \times 10^{-3}$	19.27	17.33	27.80
$3.83 \times 10^{-3}$	18.35	15.96	18.68
$2.98 \times 10^{-3}$	13.78	10.82	10.89
$2.32 \times 10^{-3}$	11.88	9.82	7.68
$1.81 \times 10^{-3}$	10.14	8.74	5.91
$1.41 \times 10^{-3}$	8.55	7.64	4.78
$1.09 \times 10^{-3}$	7.06	6.62	16.50
$8.54 \times 10^{-4}$	5.60	5.56	2.97
$6.65 \times 10^{-4}$	4.55	4.49	2.39
$5.18 \times 10^{-4}$	3.13	3.07	1.89



<u>Energy, MeV</u>	<u>SAKI</u>	<u>Jenkins</u>	<u>Doran</u>
$4.04 \times 10^{-4}$	1.10	1.02	0.17
$3.14 \times 10^{-4}$	0.0	0.0	0.19
$2.45 \times 10^{-4}$	0.0	0.0	0.21
$1.91 \times 10^{-4}$	0.0	0.0	0.24
$1.48 \times 10^{-4}$	0.0	0.0	0.27
$1.15 \times 10^{-4}$	0.0	0.0	0.30
$1.00 \times 10^{-4}$	0.0	0.0	0.32
$9.90 \times 10^{-5}$	0.0	0.0	0.0